Geothermics 135 (2026) 103522

Contents lists available at ScienceDirect

Geothermics

journal homepage: www.elsevier.com/locate/geothermics

Assessing thermal regime variability in the San Francisco Basin (Argentina): Heat flow and geothermal gradient anomalies derived from hydrocarbon exploration well data

J.P. Villalba Ulberich [a,b,*], Y.J. Peralta Arnold [a,b], M. Taussi [c], P.J. Caffe [a,b], F. Tassi [d,e]

[a] Instituto de Ecorregiones Andinas (INECOA), Universidad Nacional de Jujuy, CONICET, Av. Bolivia 1661, 4600, San Salvador de Jujuy, Jujuy, Argentina
[b] Instituto de Geología y Minería, UNJu, Av. Bolivia 1661, 4600, San Salvador de Jujuy, Jujuy, Argentina
[c] Dipartimento di Scienze Pure e Applicate, Università degli Studi di Urbino Carlo Bo, Via Ca' Le Suore 2/4, Urbino, Italy
[d] CNR-IGG Istituto di Geoscienze e Georisorse, Via La Pira, 450121 Firenze, Italy
[e] Dipartimento Scienze Della Terra, Università di Firenze, Via La Pira, 4, 50121 Firenze, Italy

ARTICLE INFO

Keywords:
Foreland basin
Geothermal gradient
Thermal conductivity
Heat flow
Thermal Source
Geothermal reservoir

ABSTRACT

The Santa Bárbara (SB) mountain range (Andean foreland, northern Argentina) has become increasingly significant in recent years for geothermal exploration, due to the presence of several hot and mineral springs with outlet temperatures of up to 40–60 °C. In this study, bottom-hole temperatures (BHT) from 24 oil wells located within the San Francisco Basin (north of Santa Barbara) were utilized to assess the thermal flow and to investigate the origin of the thermal anomalies. The BHT values, ranging from 44.4 °C to 220.2 °C, indicate a geothermal gradient ranging from 24.9 to 40 °C, a heat flow between 97 and 153 mW/m^2, and a thermal conductivity of 3.49–4.27 W/mK for the main reservoir unit (Yacoraite Formation). The derived geothermal and geological units, in conjunction with 2D seismic lines and topographic data, were utilized to map relevant structural variations, changes in thickness, and major lithological units. The conceptual model identified the northeastern and southwestern regions as two areas of equal potential for medium- to high-temperature fluid resources. The calculated 'heat-in-place' (HIP) values confirm the substantial geothermal potential of the Yacoraite Formation within the San Francisco Basin by indicating the presence of significant stored thermal energy. The findings of this study demonstrate that integrating well logging and space data with geospatial techniques is an effective method for geothermal prospecting in geological and tectonic settings within foreland environments.

1. Introduction

The sub-Andean belt of northwestern Argentina was a major center of hydrocarbon exploration in the 20th century (Yrigoyen, 1993; Vergani et al., 2008). However, as global attention focuses on climate change and reducing GHG emissions from fossil fuels, interest in renewable energy alternatives is growing. Geothermal energy has the potential to provide long-term baseload power and heat, while reducing GHG emissions and serving as a sustainable and reliable energy source, crucial for the transition to a zero-carbon future (Fàbrega Ferrer, 2022; Rahman et al., 2022; Nguyen et al., 2024). It generates baseload electricity, achieving an average capacity factor of 85 %. (Zarrouk and Moon, 2014), only surpassed by nuclear power, while producing minimal emissions and avoiding dependence on rare earths (IRENA, 2024). Heat is extracted from thermal-fluid-related reservoirs or enhanced geothermal systems (EGS), such as those developed in the FORGE project (Jones et al., 2025), which enables global deployment, with 16, 355 MW currently installed in 30 countries (IEA, 2025). The main producers are the USA (3900 MW), Indonesia (2418 MW), and Turkey (1691 MW), while Latin America contributes 11 % (1700 MW), led by Mexico (963 MW) and Central America. Despite slow regional growth (1.5–2 % per year), improved regulations seek to harness Latin America's high-temperature volcanic potential for both power generation and heating (Castillo-Reyes et al., 2024). Nevertheless, the only operating high-temperature geothermal field in South America remains the Cerro Pabellón project in northern Chile, which produces 81 MWe (Taussi et al., 2019; Cappetti et al., 2021).

Numerous studies in the area have investigated the geothermal

* Corresponding author.
E-mail address: jpvillalbau@idgym.unju.edu.ar (J.P. Villalba Ulberich).

https://doi.org/10.1016/j.geothermics.2025.103522
Received 19 September 2025; Received in revised form 24 October 2025; Accepted 3 November 2025
Available online 26 November 2025
0375-6505/

potential by analyzing the chemical and isotopic composition of fluids naturally discharged from hot and cold springs in the Subandean – Santa Bárbara system (Moreno Espelta et al., 1978; Seggiaro et al., 1995, 1997; C. Invernizzi et al., 2014; Chiodi et al., 2015; Peralta Arnold et al., 2020). These data have been utilized to develop a conceptual model that describes the source regions of thermal fluids and the chemical–physical processes governing the chemistry of waters and dissolved gases during underground circulation. In the case of the San Francisco Basin, investigations have examined the origin and chemical processes of thermal waters in the Jujuy Province (Argentina) to evaluate geothermal potential (Moreno Espelta et al., 1981; Peralta Arnold et al., 2020). These authors identified shallow aquifers in the Sub-Andean Range that interact with Cretaceous to Neogene rocks, replenished by meteoric water. Reservoir temperatures exceeding 200 °C —coupled with the potential reservoir depth (~2000 m)—suggest an anomalous geothermal gradient, underscoring the area's promising geothermal viability.

The development of sustainable geothermal resources depends on the integration of dominant geological and structural characteristics with the properties of the geothermal system itself like potential reservoir rocks' temperature, permeability, and thermal conductivity (Ghassemi, 2012; Shortall et al., 2015; Jolie et al., 2021; Izadi and Freitag, 2025).

The present research aims to develop a new method for assessing geological, structural, and hydro-geochemical data related to geothermal resources in the San Francisco area, which can be utilized for evaluating geothermal potential leading to direct future exploration in the region. The proposed methodology, based on the reanalysis of seismic lines and pre-existing borehole hydrocarbon exploration data, allowed building a new and interpretation of the basin structure and a solid evaluation of the basin geothermal potential re-analysis. The present study utilizes pre-existing data from hydrocarbon exploration wells to: i) analyze variations in geothermal gradients, ii) identify potential fluid reservoirs, and iii) indirectly infer thermal conductivity from petrophysical data of sedimentary rocks pertaining to well logs occurring in the San Francisco Basin. The primary objective of the project is to identify new locations for geothermal energy resources and assess their potential. It is expected that the identification of trends and mapping of areas suitable for the installation of geothermal power plants for electricity or thermal production. provide valuable information to community planners and developers, guiding land use, urban planning, and energy resource allocation.

2. Geological regional setting

The San Francisco-Lavayén Valley is a broad syncline that separates the Eastern Cordillera from the Santa Bárbara system in north-west Argentina (see Fig. 1). This foreland basin is characterized by a wide syncline, which is limited by an SSE-trending anticline (the Zapla Range) to the east and the Santa Bárbara (SB) mountain range to the west. The latter is an NNE-trending fold and thrust belt comprising N—NNE anticlines and reverse faults (Kley and Monaldi, 2002). Both anticline systems display a westward asymmetry, characterized by gently dipping, elongated, planar back limbs and steeply dipping-to-overturned front limbs commonly intersected by eastward-dipping thrust or reverse faults. Additionally, regional reverse faults that dip westward are exposed and imaged on seismic lines (Bianucci, 1982). The Zapla anticline is significantly broader than any fold found in the SB System, with southwestward vergence. Both flanks of the Zapla anticline are intersected by reverse faults that incline towards its core. The fault along the southwest margin is not well exposed but is thought to be a significant structure (Fig. 1C and D; Kley and Monaldi, 2002).

Based on subsurface and outcrop data interpretation, the basin's stratigraphy consists of several units deposited from the Paleozoic to recent times. Of these units, the Cretaceous-Cenozoic ones have been documented as a possible geothermal reservoir in the regional context (Maffucci et al., 2015; Invernizzi et al., 2014; Peralta Arnold et al., 2020). The fluvial Ordovician Labrado Formation consists of two coarsening upward sandstone cycles formed atop subtidal plain deposits with an erosive base. This is interpreted as a relative sea-level fall during that period, with fluvial progradation over tidal deposits (Astini and Marengo, 2006). The next Ordovician unit, Centinela Formation, is composed of fine, medium, and coarse quartz sandstones organized in thick to very thick layers containing the ichnogenus Skolithos (pipe rocks). Main characteristics of this formation suggest that it represents the advancement of a high-energy deltaic system, dominated by

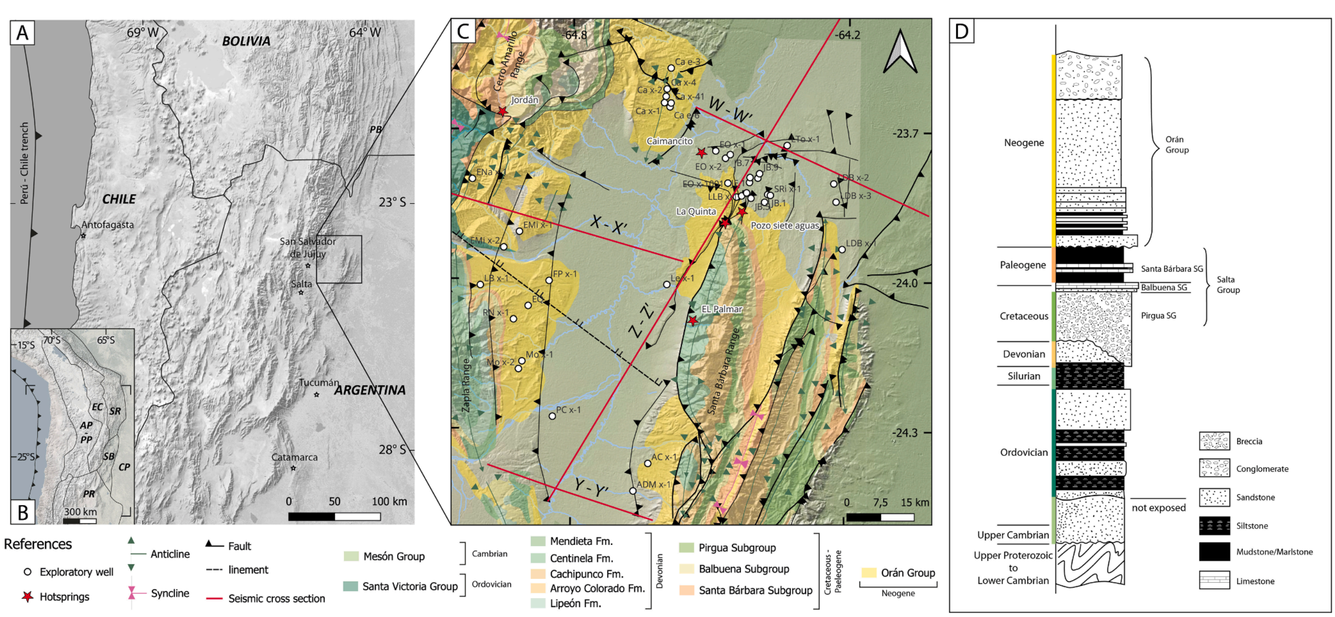

Fig. 1. **A.** The study area in the context of the Central Andes. **B.** Central Andes and the distribution of the geological provinces PR: Pampean Ranges; CP: Chaco Plain; SR: Subandean Ranges; EC: Eastern Cordillera; AP – PP: Altiplano – Puna; SB: Santa Barbara Mountain Range. **C.** Geological-structural map of the San Francisco basin (Kley and Monaldi, 2002; Ortiz et al., 2022) reporting hot springs, oil exploration wells and the traces of seismic cross sections. **D.** Simplified stratigraphy of the area (modified after Kley and Monaldi, 2002).

fluvial-influenced delta front deposits (Astini and Marengo, 2006). Silurian to Devonian sandstone and shale outcrops (Zapla, Lipeón, Arroyo Colorado, and Cachipunco formations) represent a marine sedimentary series that exhibits a general regressive trend, with proximal facies gradually displaced towards the east, and continental influence in the upper levels (Cecioni, 1949; Monaldi and Boso, 1987). These units crop out at the Cachipunco, Zapla, Centinela, and SB ranges, where an unconformity separates these rocks from the overlying Cretaceous-Paleocene strata of the Salta Group (Pirgua, Balbuena, and Santa Bárbara Subgroups), deposited during the rifting event in NW Argentina (Starck, 1995). The Pirgua Subgroup, spanning the Early to Late Cretaceous (noted in SB range), is mainly composed of red continental conglomerate and sandstone, with occasional interbedding and/or intrusions of alkaline volcanic rocks (Galliski and Viramonte, 1988; Salfity and Marquillas, 1994; Marquillas et al., 2005). The Balbuena Subgroup, dating from the latest Cretaceous to Early Paleocene comprises continental to marine sandstone, limestone, and shale (Turner, 1959). Within this subgroup, the Yacoraite Formation the Balbuena serves as the primary source and reservoir for the petroleum system in the Caimancito oilfield (Disalvo, 2002). The Yacoraite Formation is divided into lower Puesto Guardian and upper Las Avispas members, which are generally separated by a siliciclastic layer (Boll et al., 1989). The Las Avispas Member, with its higher carbonate content, is the primary reservoir of hydrocarbon resources (Boll et al. 1989). Outcrops at Cerro Amarillo reveal a 172 m sequence of well-stratified carbonates. Regionally, the base of the Las Avispas Member is represented by the "Arena 6A and 6B" sandstones in the Lomas de Olmedo sub-basin. This contact is a sequence boundary, separating the Puesto Guardian and Las Avispas members. It is interpreted as a low-stand surface, with the overlying siliciclastic and sandstone units representing incised valley fills and tidal deposits that prograde over the underlying high-stand carbonates before the subsequent carbonate deposition of the Las Avispas Member (Grosso et al., 2013). Lastly, the Santa Bárbara Subgroup, which dates from the Paleocene to Early Eocene, consists of shale with sporadic carbonate and sandstone interbeds interpreted as a lacustrine system with sporadic fluvial ingressions (Hernández et al., 1999; Starck, 2011). The Andean deposits, related to the uplift of the Puna Plateau and the Eastern Cordillera (EC), is represented by the Neogene Orán Group (Russo, 1972), which is further subdivided into the Metán and Jujuy subgroups, with most instances exhibiting an unconformable overlay on Proterozoic, Paleozoic, and Mesozoic units. The Metán Subgroup is composed of the Río Seco, Anta, and Jesús María formations (middle Miocene) which are interpreted as deposited throughout different environments, including ephemeral fluvial, eolian, and lacustrine depositional systems (Russo, 1972; Gebhard et al., 1974; Starck and Anzótegui, 2001; Quattrocchio et al., 2008 and references therein). An unconformity has been identified that separates the Metán Subgroup from the overlying Jujuy Subgroup. The latter consists of the Guanaco and Piquete formations (Gebhard et al., 1974; Russo and Serraiotto, 1978; Galli et al., 2019), which span the late Miocene to early Pleistocene (Galli et al., 2019). The Jujuy Subgroup is characterized by a dominant provenance signal derived from the EC and its paleoenvironments, which range from braided fluvial to alluvial systems exhibiting complex vertical and lateral facies changes (Gebhard et al., 1974; Russo and Serraiotto, 1978; González Villa, 2002; Hain et al., 2011; Galli et al., 2019; Villalba Ulberich et al., 2021).

The regional structure of the area is the result of a combination of Cretaceous rifting effects, subsequent thermal subsidence, and Neogene contraction. The Cretaceous rift in northwestern Argentina has a complex geometry, with four branches radiating from a central structural high (Salta-Jujuy high) toward the north, east-northeast, south, and northwest (Salfity and Marquillas, 1994). The study area occupies the NNE-trending sector that connects the Lomas de Olmedo depocenter with the Metán depocenter along the northeastern flank of the Salta-Jujuy high.

The northern boundary of the basin is defined by a transition zone between the normal foreland system north of 23°S and a fragmented system beginning south of 23.7°S represented by SB. Before the onset of rifting, erosion had deeply incised the Paleozoic succession over this arch, likely during thermal doming before the onset of rifting extension (Cominguez and Ramos, 1991; Kress, 1995), exposing Ordovician strata along its axis (Ramos, 1999). The absence and/or truncation of detachment levels in Silurian and Devonian rocks are thought to be responsible for the termination of the thin-skinned fold-and-thrust belt to the south (Belotti et al., 1995; DeCelles and Giles, 1996; Kley, 1996; Echavarria et al., 2003; Pfiffner, 2017; Horton and Folguera, 2022).

3. Hydrographic network, thermal springs, and recharge areas

The San Francisco hydric basin covers an area of 25,113 km^2. The drainage network is well-integrated and exhibits a marked structural control of a trellis to parallel pattern (García et al., 2008). Longitudinal valleys are progressively integrated toward the east by antecedent streams that transversely cut the mountain ranges. These valleys connect to the Plata Basin through the Bermejo River. The main system consists of the Lavayén and San Francisco rivers, which receive numerous tributaries from both flanks. Notable tributaries include the Capillas-Negro, Ledesma, Grande, and San Lorenzo rivers from the west, and the Santa Rita, Del Medio, and Colorado rivers from the east (supplementary material 1, García et al., 2008).

The San Francisco basin hosts unconfined and confined aquifers. The first type (Fuertes et al., 1997) belongs to the San Francisco-Lavayén Aquifer System (SFLAS, supplementary material 1), where the main recharge is made up of contributions from the Grande-Mojotoro Aquifer System. The latter contributes to the SASFL through the Aguas Calientes Strait and from there, into the Lavayén River valley from the south and from the north with contributions coming through the San Juancito Strait. From the western flank of the basin, the recharge occurs at the Zapla and Cerro Amarillo mountain range in which rainfall exceeds 1400 mm per year. At the foothills of this mountain range, heterometric alluvial deposits with a high infiltration capacity crop out. On the eastern flank, the Gallo, Centinela, and SB Mountain ranges are good recharge zones with sediments with significant infiltration capacity in the foothills (supplementary material 1).

Thermal manifestations occur throughout the study area (Fig. 1C). The main thermal springs occur in the Sub-Andean Range (El Jordán and Aguas Calientes) and in the SB mountain range (La Quinta, Caimancito, El Palmar, and Siete Aguas) (Peralta Arnold et al., 2020). These hot springs (temperatures up to 72 °C measured at Siete Aguas) are recharged by meteoric water and fed by a hydrothermal aquifer mainly hosted in the Yacoraite Formation. Besides, their emergencies are strictly controlled by tectonic structures (Peralta Arnold et al., 2020). La Quinta thermal springs show high Total Dissolved Solids (TDS >16,000 mg/L) and a Na-Cl composition, whereas El Palmar, El Jordán, Caimancito, and Siete Aguas thermal springs have a Na-SO_4(Cl) composition, coupled with lower salinity levels (992 - 4500 mg/L) (Peralta Arnold et al., 2020). Eventually, Aguas Calientes show lower temperatures (22 – 29 °C), low TDS (326–527 mg/L) and a Ca-HCO_3 composition (Peralta Arnold et al., 2020). Geothermometric applications suggested that the reservoir fluid has estimated temperatures of ~200 °C (Peralta Arnold et al., 2020).

4. Methodology

The San Francisco basin was studied for geological, stratigraphic, structural, and hydrogeological reconstruction, coupled with an analysis of the geothermal gradient to understand the geothermal potential of deep confined reservoirs. Geological studies based on surface and subsurface information were used for determining the stratigraphic limits and depth of potential reservoirs, for evaluating the properties of the different lithological units that may contain or seal geothermal fluids, as well as reconstructing the axial trend of the main folded structures, and performing preliminary structural analyses of the reservoirs associated with the thermal fluids.

4.1. Basin configuration

Remote sensing analyses were performed using Global Multi-Resolution Topography (GMRT, Ryan et al., 2009) data with a 10 m resolution and were developed by Q-GIS software. Detailed mapping of both structural elements (faults and fractures) and lithologies were obtained by combining existing geological maps and the information present in the available well logs and seismic profiles. The same dataset was exploited to reconstruct the subsurface system, by defining the thickness, distribution, and depth of the lithologies present, as well as the presence of confined aquifers.

The structural model integrated 2D seismic data with borehole information from ten wells to constrain the geometry of the Salta Group and validate the structural interpretation (Fig. 3). Twenty-two seismic lines combined in four transects provided a comprehensive E-W and N-S understanding of the basin's structure and stratigraphic development. The model was carried out in MOVE software (Midland Valley company) with an academic license from National University of La Plata.

4.2. Temperature database

The geothermal gradient of the San Francisco basin was calculated based on temperature measurements taken from exploration boreholes drilled between the 1930 and 1990 and available at the Jujuy Provincial Secretariat of Mining and Hydrocarbons. Based on exploratory well files, we made a database of bottom hole temperatures (BHTs) and drill stem test (DST) temperature records. The maximum temperature registered for each well can be considered the real formation temperature. The resulting dataset consists of about 49 single values (from BHTs) derived from 24 Wells, and continuum measurements of DST in 2 wells. The dataset was carefully filtered to ensure the highest level of reliability, considering the age of the information.

Downhole temperature measurements are important for accurately determining the thermal profile in wells. These measurements are crucial for estimating the undisturbed formation temperature, which is paramount in geothermal exploration and reservoir engineering (Grant, 2013). To estimate the true equilibrium temperature, all the data used in this work were adjusted to account for thermal anomalies caused by drilling activity. Post-drilling temperature readings from deep wells provide a comprehensive dataset, but these temperatures are affected (up to 10 %) by the drilling process, specifically by the cooling effect of mud circulation (Waples et al., 2004a). Adjustments to the data are only feasible for downhole temperature logs, depending on the acquisition of a series of measurements.

The correction of log-derived bottom-hole temperatures has been significantly improved by relatively recent pioneering research (Waples and Ramly, 2001; Waples et al., 2004a,b). These authors formulated equations for correcting bottom-hole temperatures based on log data from three geologically different basins.

When multiple time-temperature data are available, the main practical issue with applying the Horner plot correction, is that information on time since end of circulation (TSC) is almost always unavailable. Various authors have circumvented this issue by using a standard circulation time for all corrections. For example, Chapman et al. (1984) and Reiter and Jessop (1985) used 4 h, while Deming and Chapman (1988) used 5 h. The apparent justification for this practice is that it can easily be demonstrated that the equilibrium temperature predicted by the Horner plot varies little as the assumed circulation time changes. However, this does not demonstrate that the accuracy of the Horner plot is unaffected using incorrect circulation time. Nevertheless, Luheshi (1983) has shown that temperature build-up in a well is relatively insensitive to circulation time duration. Scott (1982) studied Canadian wells for which circulation times were given and found a mean circulation time of 8 h, a median of 3 h, and a standard deviation of 13 h. This indicates that, although a standard circulation time of 4 or 5 h is probably reasonable, situations in which the actual circulation time is up to 30 or 40 h may not be uncommon. To address this issue, Waples et al. (2004a) determined the TSC based on a function of measurement depth as follows:

$$TSC = 0.0465 * Z^{0.7} \quad (1)$$

We carried out a correction of the borehole measurements based on this equation, because the wells' data used did not present TSC values.

4.3. Thermal conductivity and heat flow calculation

The availability of subsurface rock samples limits the quality of thermal model parameters beyond specific geological formations. This leads to uncertainty in model results as input data often falls below the capabilities of numerical tools. However, some methods accurately represent the thermal characteristics of subsurface rocks using borehole geophysical logs (Blackwell and Steele 1989; Brigaud et al. 1990; Demongodin et al. 1991; Fuchs and Förster, 2010, S. 2014). These methods are limited because equations for thermal conductivity prediction are only validated for specific rocks and localities. Changes in rock composition affect the relationships between thermal and petrophysical properties (Kukkonen and Peltoniemi, 1998), making it challenging to develop universally applicable equations for all sedimentary rocks. Therefore, researchers tend to restrict empirical equations to specific rock types and geographical regions. To overcome this limitation, S. Fuchs and Förster (2014) proposed a method that combines laboratory measurements with downhole logging data to improve the accuracy of thermal models and overcome the need for specific rock samples.

To address limitations in predicting rock properties, S. Fuchs and Förster (2014) developed prediction equations based on a comprehensive dataset of synthetic rock compositions. These equations can be applied to different well logs and descriptors combinations, such as bulk density, shale volume fraction, neutron porosity, sonic transit time, and photoelectric absorption rate. The equations were established for three main sedimentary rock groups (clastic rocks, carbonates, and evaporites) using large sets of synthetic rocks with different compositions. The original purpose of these equations was to calculate total organic carbon (TOC), but they have been enhanced to consider varied porosity and extended to include three thermal features. The rock property values obtained from these equations consider the influence of the mineral matrix and pore-filling fluid (water). Statistical analysis based on these values leads to the development of accurate prediction equations for the desired rock properties. Because of the lack of laboratory measurements of the thermal conductivity of the rocks occurring in the study area, it was necessary to estimate this property through indirect measurements. The thermal conductivity and the heat flow calculations were thus performed on downhole logging for the Yacoraite Formation, which is the primary focus of the exploration, considering the entire unit as a carbonate lithological unit. Based on these data and following the methodology of S. Fuchs and Förster (2014) and Fuchs et al. (2015), the thermal conductivity (λ) was determined using the Eq. (2):

$$\lambda = 5.84 - 0.0063\,\Delta T - 1.48\,Vsh \quad (2)$$

This equation allows the calculation of λ based on shale volume (Vsh = (GR - GRmin) / (GRmax - GRmin)) and the sonic log (ΔT). This method was chosen because it provides the most accurate prediction of λ when ΔT and Vsh are combined (R^2 of 0.767 and SD of 9.8 %, Fuchs et al. 2015).

4.4. Geothermal mapping

The interpolation of geothermal gradients from individual well data and the generated heat flow maps were carried out using the SAGA multilevel b-spline algorithm of Q-GIS software. This is the first time this approach is applied for geothermal gradient and heat flow mapping., at the best of our knowledge. The target unit was the top of the Yacoraite Formation since it serves as the reservoir proposed in prior research (Peralta Arnold et al., 2020) and represents the bottom of the exploration wells, as it was also the designated target for previous hydrocarbon exploration activities (Disalvo, 2002). In the first step, outlier values that generated anomalous alterations and were inconsistent with those expected for the study area were discarded. For example, gradient values above 80 °C/km or below 10 °C/km were removed, while an arithmetic mean was calculated for wells with more than one gradient value in those cases where the variations between individual gradients did not exceed 10 %.

The geothermal gradient map was then used to calculate the temperature distribution for the top of the Yacoraite Formation. The benefit of this approach over constant depth temperature mapping is that the resulting maps combine two aspects relevant to geothermal exploration: temperature and geology. Structure-depth maps were calculated for the Yacoraite Formation using well-control data, applying the ordinary kriging algorithm.

5. Results

5.1. Basin configuration

The new structural analysis performed in this present study shows that the basin exhibits a typical development of Andean basins, elongated in a N-S direction, with an eastward rotation in the northern sector due to the influence of pre-existing structures from the Salta Rift (Fig. 1). The geometries of the deep structures reflect a predominance of inverted normal faults with a N-S orientation across most of the basin, with their maximum expression in the Zapla and SB ranges, which border the basin on both margins.

Additionally, based on W-E structural cross-sections (Fig. 3A, B, C) and starting from the top of the Yacoraite Formation, an increase in the thickness of the entire Salta Group can be observed toward the east and north. This increase is associated with the thinning and absence of the

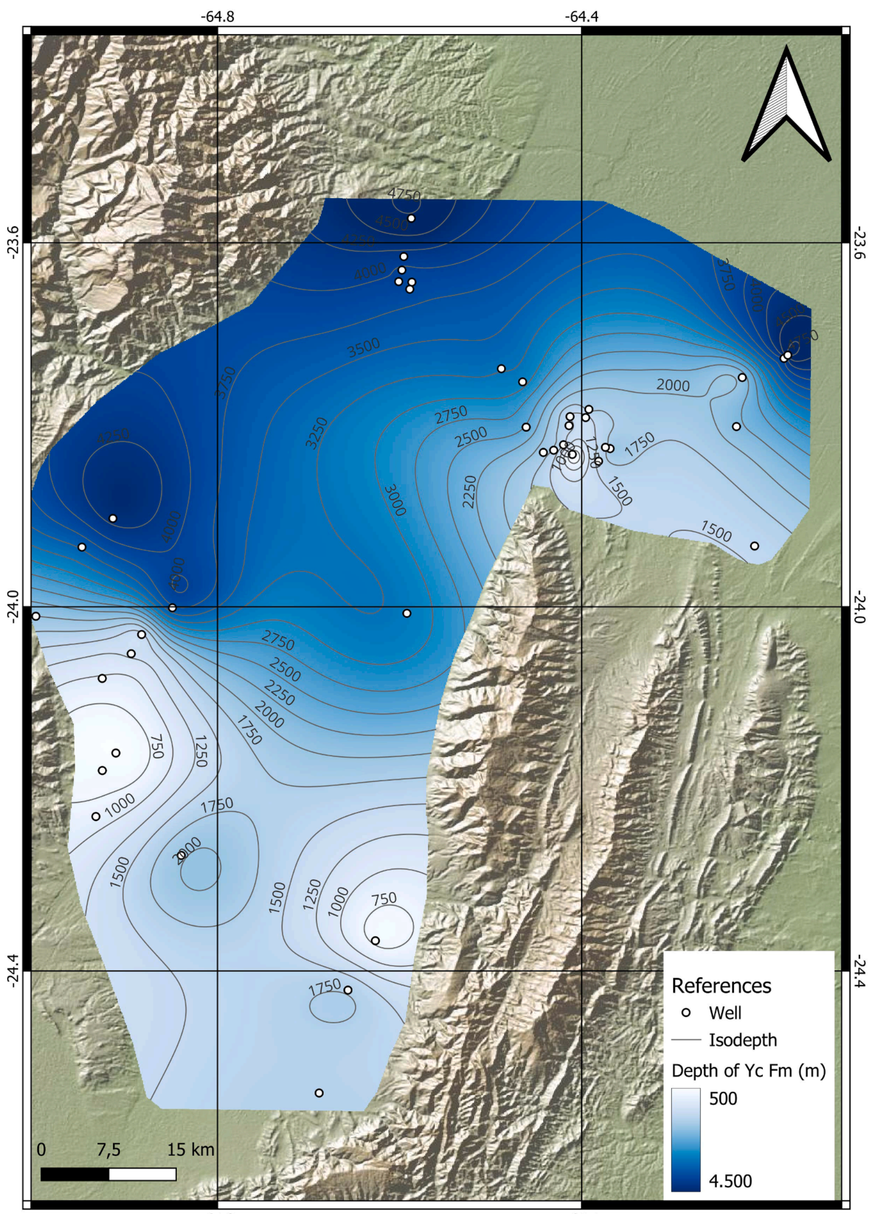

Fig. 2. Structural map of the top of Yacoraite Formation.

Pirgua Subgroup and the Lecho Formation toward the southwest, as well as a reduction in thickness of the Yacoraite Formation in the same direction (Fig. 3D). Fig. 2 shows a structural map of the top of the Yacoraite Formation, which exhibits a structural jump in the central sector of the basin with an NW-SE orientation. This structural feature influences the development of both the Salta Group and the Cenozoic foreland fill, thickening them towards the north. When this structure is analyzed through seismic data (Fig. 3), several structural jumps with an NW-SE orientation can be observed, which tend to deepen Yacoraite Formation in most cases. The Cerro Amarillo and Zapla mountain range emerges to the west of the basin. In this sector, Andean compressive tectonics exposed both Paleozoic and Mesozoic units, causing the shallowing of the tops of the Mesozoic formations.

In summary, the thickness of the Yacoraite Formation in the entire basin ranges from 16 m to 350 m, with an increasing thickness trend toward the northeast (Fig. 3D). In the northeastern sector of the basin, the thickness is predominantly >200 m, coincidently with the deepening and thickening of the rift basin.

5.2. Data wells, temperatures and hydrochemistry

We have recognized several confined water reservoirs using boreholes records (Table 1), for which highly variable thicknesses, ranging from 1 to 70 m, are documented, likely representing the geothermal water reservoirs. In the southern and western sectors, where the foreland deposits and the Salta Group are either thin or absent, the main confined water reservoirs lie primarily in Paleozoic strata, predominantly composed of Paleozoic quartzites. The Centinela and Arroyo Colorado Formations stand out among those. The Centinela Formation shows variable thicknesses ranging from 450 to 1000 m in outcrops (Monaldi et al., 1986), while well data indicate thicknesses between 350 and 630 m. It consists mainly of quartzites, with porosities averaging 11 % in the AC X-1 well (Fig. 1C; Table 1). Water characteristics include salinity values of 7500 ppm and flow rates between 5 and 54 m^3/h (Qdo X-2, Table 1).

Toward the north and east, the Salta Group thickness and the foreland deposits increase significantly, often exceeding 1000 m, with the Salta Group located at depths > 2500 m below the surface (except at the basin edges). In this area, where well data do not reach the Paleozoic terrains (located 5000–6000 m below the surface), the aquifers are concentrated in Mesozoic and Cenozoic units.

We have documented confined reservoirs in three wells in the Pirgua Subgroup, including well JB 5, which contains records of up to three aquifers within the subgroup. These aquifers have a thickness of up to 2 m and flow rates >1400 m^3/d. (Table 1).

In the Balbuena Subgroup, confined aquifers are found in the Lecho, Yacoraite, and Olmedo units. The Yacoraite Formation, primarily composed of carbonates (averaging 61 %), followed by mudstones and minor sandstones, is the unit with the most confined aquifers recorded in exploratory wells. Particularly, the upper member of the Yacoraite Formation, averaging 89 m in thickness with a silt-clay basal level, serves as the primary carbonate reservoir identified in the area (Grosso et al., 2002). This reservoir may correspond to those documented in the boreholes Ca e-3, EO X-1, LDB X-1, LDB X-3, SJD X-1, LBE X-1, and AC 1.

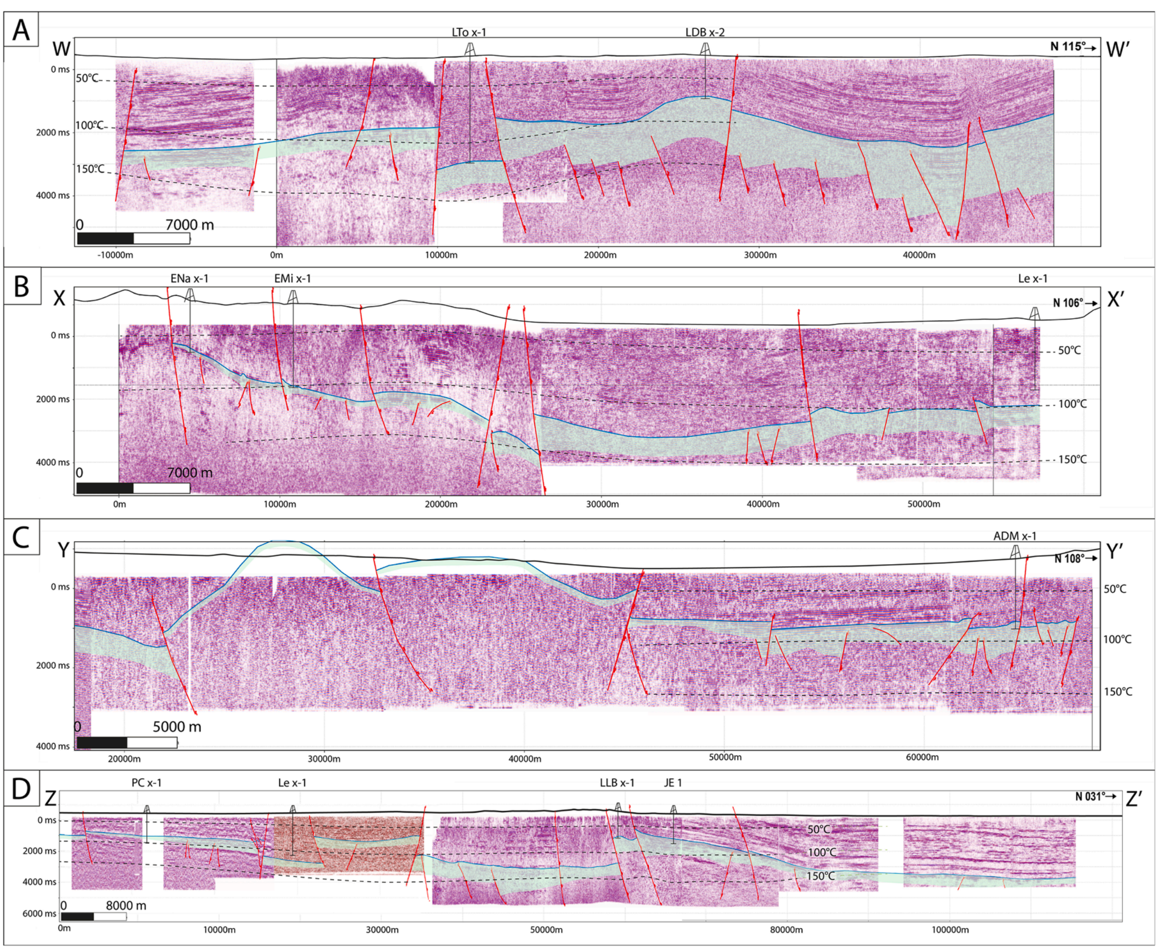

Fig. 3. Seismic cross sections (location in Fig. 1) from west to east (A, B and C) and from south to north (D). The green color shows the thickness from the top of Yacoraite to the base of the Pirgua sinrift subgroup, while the red lines are the interpreted faults. Black dashed lines represent the inferred isotherms. Trace lines are reported in Fig. 1C.

Table 1
Recognized water reservoirs from well data. In column age: 1, Devonian; 2, early Cretaceous; 3, Late Cretaceous; 4, Cretaceous-Paleogene; 5, Paleogene; 6, Miocene-Pliocene.

Well name	Geological unit	Age	Reservoir thickness (m)	Depth (m)	Porosity (%)	Flow rate (m^3/d)	Salinity (ppm)	Temp (°C)
Qdo X-2	Centinela	1	4	589	-	1296	-	-
Ca e-3	Pirgua	2	16	4799	-	-	97,420	-
Ca e-3	Pirgua	2	22	4759	-	-	97,780	-
JB 5	Pirgua	2	-	878	-	1032	4160	65
JB 5	Pirgua	2	2	1040	-	0.05	74,200	35
JB 5	Pirgua	2	1	1083	-	1440	82,020	70
JE 1	Pirgua	2	2	1923	-	254.4	87,300	-
ADM X-1	Lecho	3	40	1738	-	-	96,600	-
AC X-1	Yacoraite	4	12	727	-	300	93,580	-
Ca e-3	Yacoraite	4	13	4443	-	408	98,100	-
Ca e-3	Yacoraite	4	1	4711	6	-	97,440	-
Ca X-41	Yacoraite	4	1	3899	-	288	66,500	-
EO X-1	Yacoraite	4	30	3243	8	-	97,420	-
EO X-2	Yacoraite	4	-	3138	-	-	98,480	-
JE 1	Yacoraite	4	-	1617.5	-	-	95,980	
JE 1	Yacoraite	4	1	1660	-	0.96	92,800	-
JB 1	Yacoraite	4	2	1512.6	-	0.79	95,100	75
JB 1	Yacoraite	4	2	1536	-	5.04	92,380	75
LDB X-1	Yacoraite	4	28	1587	15.5	288	-	-
LDB X-2	Yacoraite	4	6	2178	8.5	7.88	6400	-
LDB X-3	Yacoraite	4	70	2140	9	6.94	2500	-
Mi X-2	Yacoraite	4	6	3533	7	270	80,920	-
Qdo X-2	Yacoraite	4	6	536	-	480–1200	-	-
SJD X-1	Yacoraite	4	40	1668	17.5	-	7800	-
LBE X-1	Yacoraite	4	47	1586	10	-	97,500	-
JE 1	Yacoraite	4	5	1617	-	6.48	95,980	-
JE 1	Yacoraite	4	1	1660	-	0.96	92,800	-
AC 1	Yacoraite	4	27.1	691.9	-	477	-	
Ca X-41	Olmedo	4	1	3853	17	31	54,000	-
EO X-1	Mealla	5	7	2951	12	-	94,200	-
JB 5	Mealla	5	9	530	-	0.72	53,980	55
JB3	Mealla	5	-	895	-	-	97,200	52
Qdo X-2	Mealla	5	5	341	-	-	-	-
Qdo X-1	Mealla	5	3	541	-	-	-	-
JB 3	Mealla	5	9	1030	-	-	97,380	40
JE 1	Maíz Gordo	5	3	923	-	-	95,720	51
Ca X-41	Maíz Gordo	5	3	3097	4.5	1.3	62,000	-
JB 1	Maíz Gordo	5	-	450	-	10.8	89,740	50
Ca e-3	Lumbrera	5		3968	-	-	66,160	-
Ca X-1	Lumbrera	5	9	3136	-	-	-	-
Ca e-3	Orán	6	-	2882	-	-	34,980	-
JB 3	Orán	6	-	105	-	-	-	-
JE 1	Orán	6	3	125	-	720	93,760	-
JE 1	Orán	6	3	191	-	1200	93,460	-
JE 1	Orán	6	1.70	248.8	-		84,180	
Mi X-1	Orán	6	-	520	-	81.6	4250	-

As the target unit for hydrocarbon exploration, it has undergone more intensive testing and therefore provides most of the data. We have recorded evidence of at least 18 confined aquifers across 14 wells (Table 1). Some wells, such as Ca e-3 and JB 1, record two confined aquifers, while the JE 1 well records four in Yacoraite Formation. The aquifers occur at depths ranging from 690 to 4700 m below the surface. The Lecho and Olmedo Formations instead only record isolated aquifers.

In the Santa Bárbara Subgroup, well data confirm at least 11 confined aquifers distributed across the Mealla, Maíz Gordo, and Lumbreras Formations. JB-3 well records two confined aquifers within the Mealla Formation. The highest flow rates occur in the Maíz Gordo Formation, with values of 10 m^3/d (Table 1, JB 1).

Finally, confined aquifer levels in the Cenozoic foreland deposits have been also identified, with high flow rates reaching up to 1200 m^3/d at depths between 125 and 2900 m below the surface (Table 1).

The chemical characteristics of the aquifers were investigated by analyzing 18 water samples from various formations (see supplementary material 2, Fig. 4). While most of the waters are Na-Cl types (Fig. 4C), some compositional variations can be observed (Fig. 4). Generally, most samples show relatively high concentrations of both Ca^{2+} and SO_4^{2-} (Fig. 4). The sample from well Mi x-2 (sample 14, Fig. 4) contains significantly more Mg^{2+} and Cl^- relative to the others and corresponds to waters occurring in the Yacoraite Formation. Samples from the different aquifer horizons found in well JB5 (samples 1, 2, 3, 4, and 16, Fig. 4) indicate that the shallowest ones (at a depth of ~600 m in the lower Mealla and upper Pirgua formations) are characterized by waters dominated by bicarbonate, with increased chloride content. The Na^+ versus Cl^- plot suggests that the waters found in the Pirgua, Lumbrera, Orán and Lecho formations show evidence of halite dissolution (Fig. 4B). Additionally, gypsum dissolution is evident in the Lumbrera Formation (sample 17, Fig. 4) and in sample EO X-2 (sample 9, Fig. 4) of the Yacoraite Formation.

5.3. Geothermal gradient

Using 49 BHT (Bottom Hole Temperature) data points from 21 wells, we applied the temperature correction reported in Eq. (1) (Waples, 2004a). We observed an increase in temperatures of approximately 21.55 % (min. of 15.75 % and max. of 27.45 %), with a standard deviation of 3.04 (Fig. 5). Additionally, we assumed an average ground temperature of 23.76 °C, derived from a series of measurements taken at 10 cm below ground level at the Palma Sola meteorological station during the 2013–2024 cycle (cf. INTA, https://view.officeapps.live.com/op/view.aspx?src=https%3A%2F%2Fsiga.inta.gob.ar%2Fdocument%

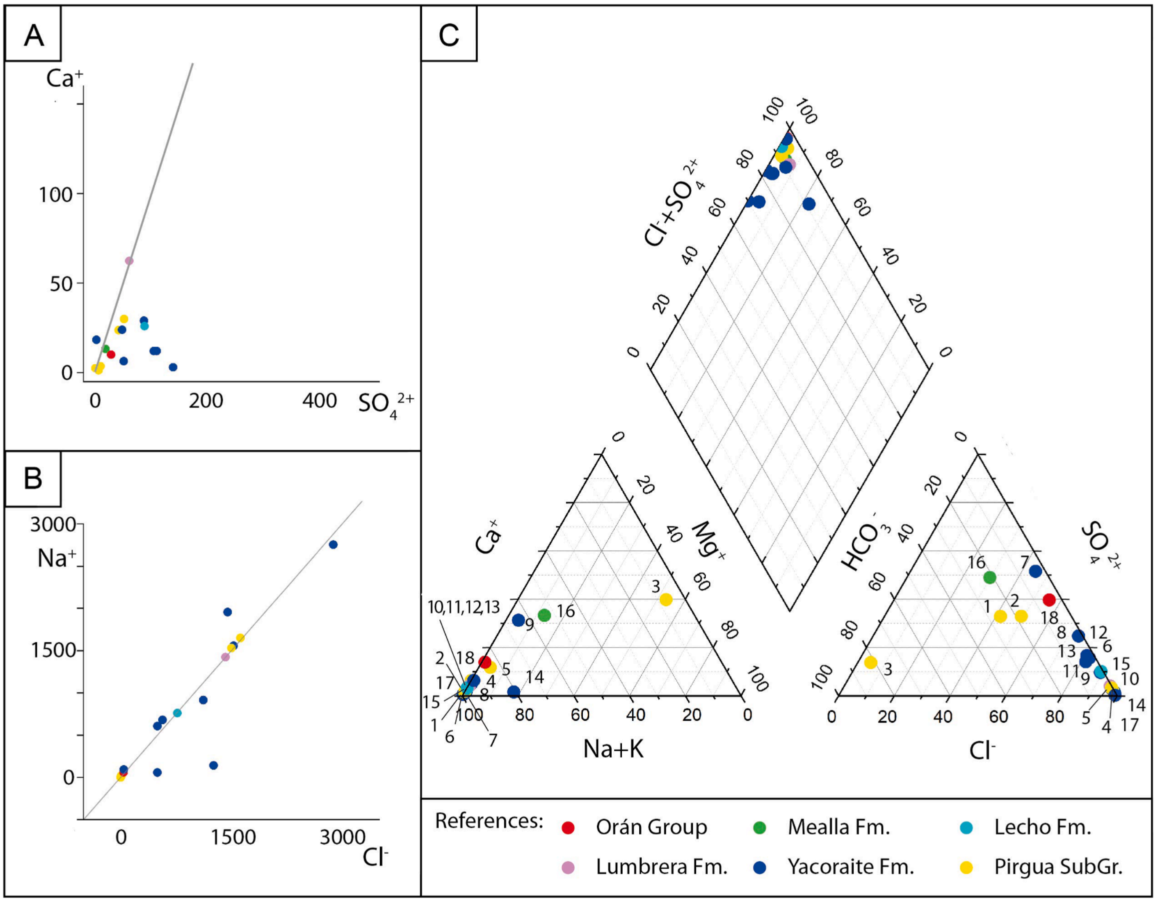

Fig. 4. A depiction of the chemical characteristics of the aquifers. **A.** Ca^{2+} versus SO_4^{2-} plot of water data. **B.** Na^+ versus Cl^- plot of water data **C.** Piper diagram. Dataset in the supplementary material 2.

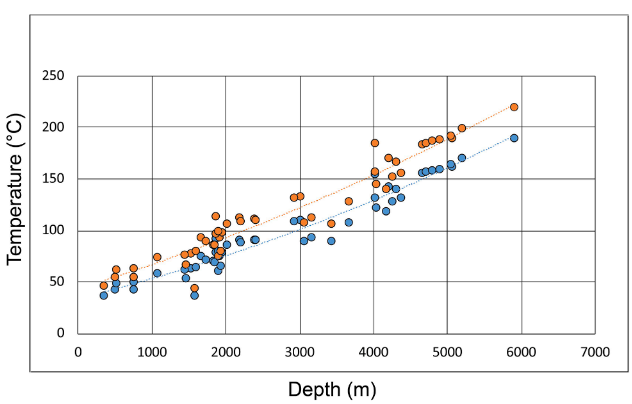

Fig. 5. Bottom Hole Temperature (blue) and Corrected Bottom Hole Temperature (orange) plotted versus depth for the San Francisco basin wells.

2Fseries%2FA872882.xls&wdOrigin=BROWSELINK).

We determined 21 individual gradients from corrected BHT measurements and two data points from corrected continuous measurements (DST). These results yielded an average gradient for the basin of 33.29 °C/km, with a minimum value of 24.13 °C/km in the Fraile Pintado well (FP X1 in Table 1) and a maximum value of 40.62 °C/km in the Santa Rita well (SR X1 in Table 1; Fig. 6). Based on these results, we created a gradient distribution map for the basin, shown in Fig. 6. The map reveals a central-northern region where gradients are predominantly below the average. In contrast, values above the average are concentrated in the south, central-west, and northeast of the basin.

Additionally, the temperature at the top of the Yacoraite Formation is illustrated in Fig. 6B, which clearly shows potential temperatures at which this unit could function as a reservoir. In the central sector of the basin, a temperature increase toward the north is observed, resulting from a rapid deepening of the unit, as highlighted in the depth map of the Yacoraite Formation's top (Fig. 2). The coldest temperatures correspond to the basin edges, where the units tend to crop out, and to the central sector of the basin, where the top of the Yacoraite Formation exhibits a temperature decrease in an ENE-aligned zone, with temperatures ranging between 25 °C and 50 °C.

Temperatures exceeding 100 °C occur in the NW sector of the basin. By contrast, temperatures below 100 °C were recorded in the southwestern and central western sectors of the Arroyo Colorado Formation, which are separated by the aforementioned ENE lineation (Fig. 2). The highest temperatures are found in areas where the Salta Group deposits are deepest, which correspond to the deepest parts of the basin in the NW sector. Here, temperatures exceed 180 °C at depths of ≥4.5 km (Fig. 2 and 6B).

5.4. Heat flow

We calculated the heat flow from the basin using exploratory wells with well logs for the carbonated interval associated with the Yacoraite Formation, on the condition that this formation contained >50 % carbonate. For the purposes of this study, the Las Avispas Member of the carbonate-dominated section of the Yacoraite Formation was selected. As the volume of shale is contingent upon the presence of gamma rays (GR), a suite of 12 wells was selected, each characterized by GR and ΔT logs. The selection was also based on the lithology content of the

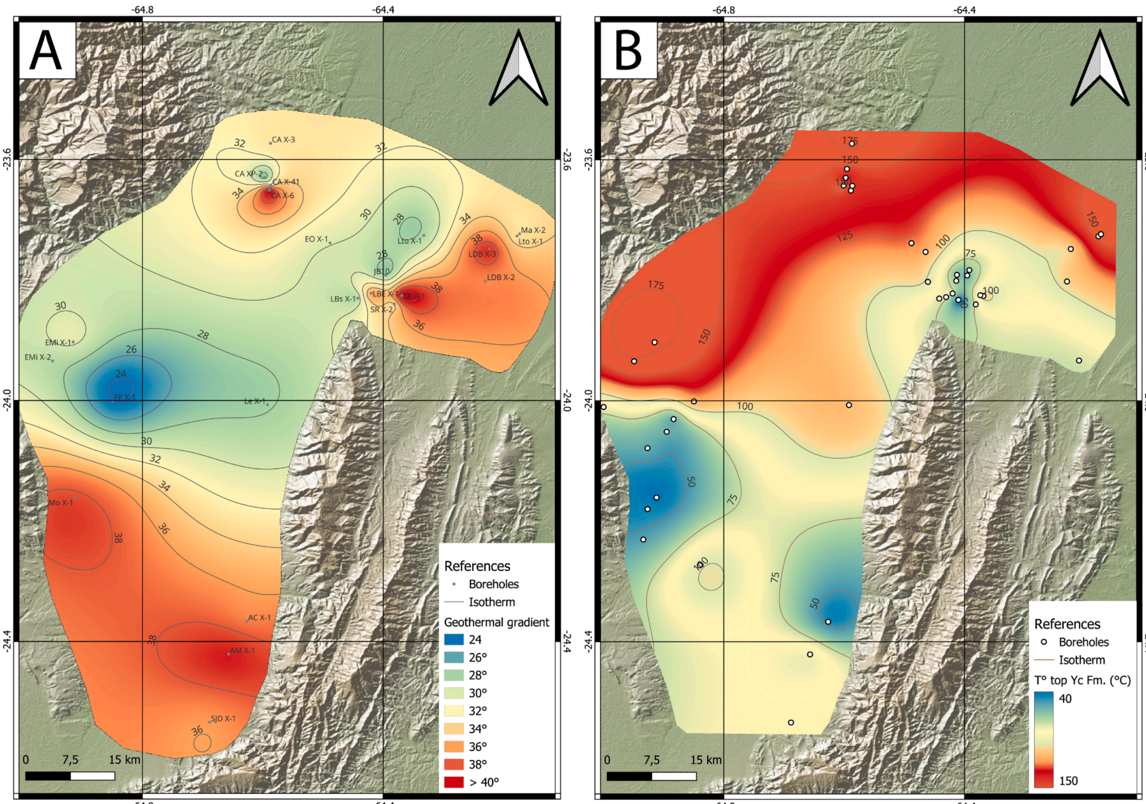

Fig. 6. **A.** Spatial distribution of geothermal gradient measurements derived from oil exploration wells at the San Francisco basin. **B.** Temperature at the top of Yacoraite Formation.

boreholes (Table 2), which show a mean of 65.6 % carbonates, 25.7 % shales, and 8.7 % sandstones, for the Yacoraite Formation, and a mean of 76.3 % carbonates, 21 % shales, and 2.7 % sandstones for the Las Avispas Member. A thermal conductivity value was determined for each tested meter of the LA Member Las Avispas Member and then averaged over the entire thickness of the unit to obtain a single, homogeneous value for the formation in each well. As a result, 12 λ values were obtained (Fig. 7A), with an arithmetic mean of 3.99 W/mK (SD = ±0.26), with a maximum value of 4.32 W/mK in the Ma X-2 well, consistent with significant carbonate development, and a minimum value of 3.58 W/mK in the CA XP-41 well. Despite the absence of analogous unit values in the region with which conducting a comparative analysis, some authors have estimated regional λ values, which confirm a certain degree of similarity with the estimated values (Henry and Pollack, 1988; Springer, 1999; Vieira and Hamza, 2014; Ibarra et al., 2021).

The heat flow (HF) was calculated using the Pascal (2015) Eq. (3):

$$HF = -\lambda \cdot \partial T / \partial z \tag{3}$$

where HF is the heat flow, λ is the thermal conductivity, *T* is the temperature and *z* is the depth noted positive downwards. Based on the obtained λ values, in which heat flow (HF) is directly related to thermal conductivity and the geothermal gradient. The results, shown in Fig. 8A, B, indicate HF values with an average of 124.8 mW/m^2 (SD = 11.04), with a maximum value of 142.36 mW/m^2 in the LTo X-1 well and a minimum value of 110.04 mW/m^2 in the Mi X-1 well.

Similar to the geothermal gradient, a HF map was created to analyze spatial variations across the basin (Fig. 8C). The map shows an increase in HF toward the southern sector, consistent with the higher temperature gradients observed in that area. Finally, it is important to clarify the advantages and limitations of this methodology. As other authors have pointed out (Brigaud et al., 1990; Förster et al., 1997; S. Fuchs and Förster, 2014), estimating λand HF from well data enables these

Table 2
Lithological variability of Yacoraite Formation and Las Avispas Member in the investigated boreholes. λ expressed in W/mK.

	Yacoraite Fm.			Las Avispas Member			Arithmetic mean λ (Las Avispas Member)
	Sandstones	Shales	Carbonates	Sandstones	Shales	Carbonates	
Ca xp-41	1	25.1	73.9	0	9.9	90.1	3.58
LBE X-1	22	42	36	7.7	17	75.3	4.18
LBs X-1	17.9	5.1	77.1	1.1	13.2	85.7	4,20
Lto X-1	12.3	29.9	57.8	6.9	8.4	84.7	4.32
Mo X-1	0	7	93	0	7	93	3.67
Ca X-4	4.6	18.4	76.9	2.5	19.8	77.7	3.65
EO X-2	4.4	20.2	75.4	3.1	16.2	80.7	4.07
Mi X-1	0	23	77	0	23	77	3.81
EO X-1001	19.4	6.7	73.9	0	16.8	83.2	3.96
LB X-1	11.1	39.8	49	1.7	38	60.4	3.99
Ma X-2	10.9	48.4	40.7	8.4	40.5	51.2	4.32
Ca X-6	1	42.2	56.7	1	42.2	56.7	4.16

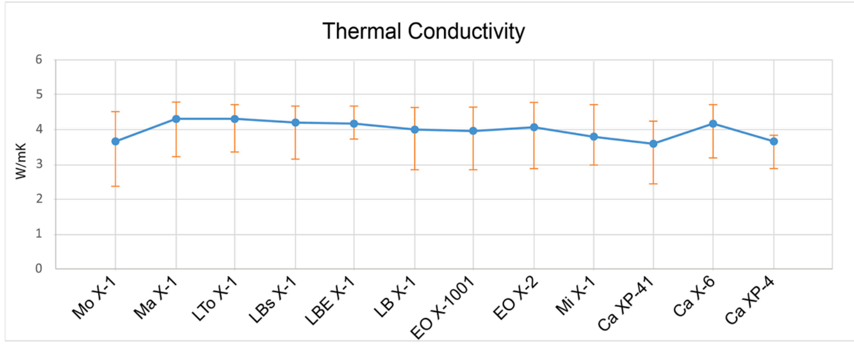

Fig. 7. Thermal conductivity calculated from well-logging.

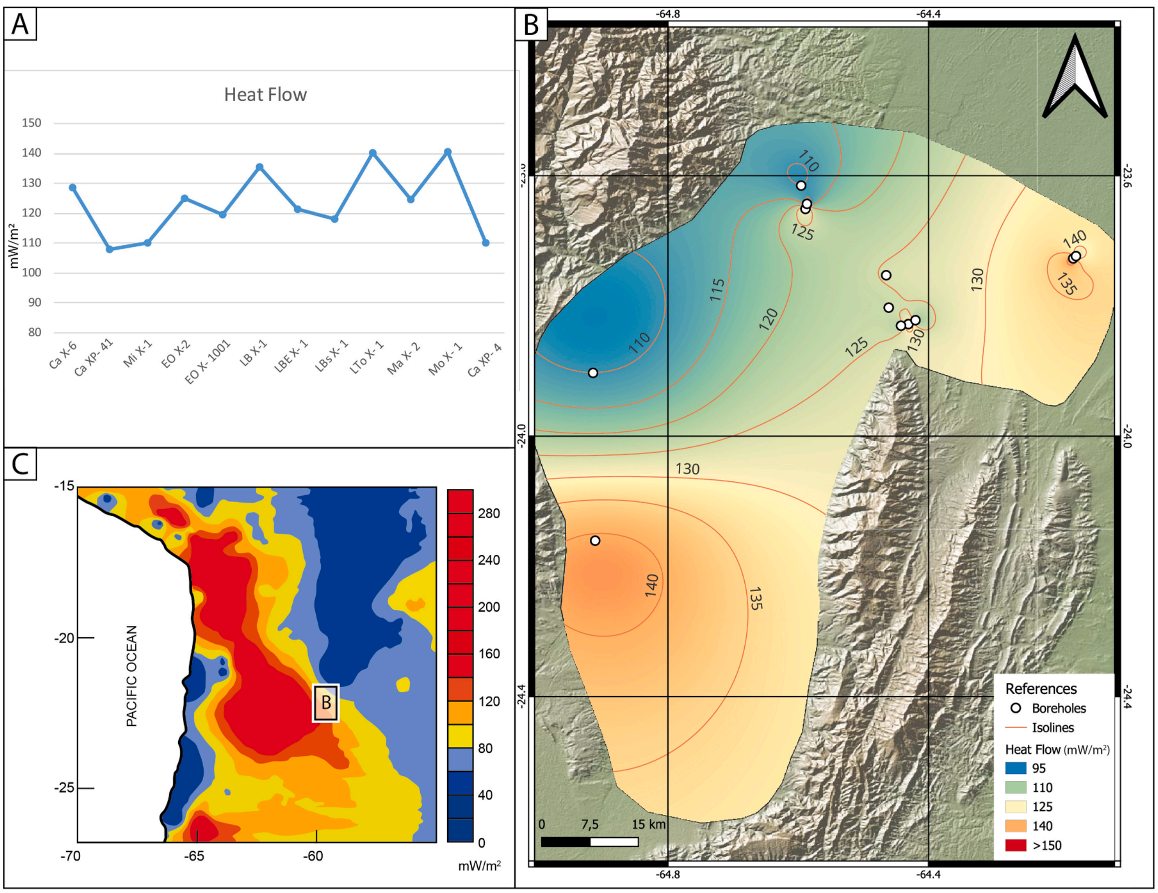

Fig. 8. A. Individual heat flow from Yacoraite Fm (Las Avispas Member). **B.** Heat flow of Yacoraite Formation (Las Avispas Member) in the San Francisco basin. **C.** Regional heat flow modified from Hamza et al. (2005).

properties to be determined under real porosity and water saturation conditions, as reflected in well logging. However, the quality, age and representativeness of the data, particularly the temperature measurements, can introduce limitations. In addition, the future collection of new geothermal gradient measurements and in situ λcalculations may contribute to the validation and refinement of the model.

6. Discussion

6.1. Basin configuration

The review and reinterpretation of data from well logs and previous studies of the San Francisco Basin allowed to infer that the primary deformation mechanism shaping the basin is the inversion of high-angle structures from the Salta Rift, combined with thermal subsidence and Neogene contraction associated with the uplift of the Andes. These structures gave rise to a system of inverted blocks, primarily along the basin margins, where the largest vertical displacements can be observed. Most of the thermal springs documented by Peralta Arnold et al. (2020) are associated with the Santa Bárbara Fault, a major structure of the Cretaceous rift that is now inverted, for which an extension of up to 10 km deep has been estimated (Kley and Monaldi, 2002; Ortiz et al., 2022). This structural configuration plays a dominant role both in the formation of the basin and the development of the fluid migration pathways, which are more pronounced in the northern sector.

The structural-stratigraphic analysis demonstrates the occurrence of an ENE-WSW-trending rift structure, which marks a boundary in the development of geothermal fluid reservoirs to the north and south. This structure, a normal fault with a displacement of at least 1500 m (see Fig. 3D), controls two key aspects: (1) the extent and development of the Yacoraite Formation and the Salta Group, preventing favorable development of its basal levels (Pirgua and Balbuena Subgroups) toward the south; and (2) the depth of the Meso-Cenozoic reservoirs is <1000 m to the south, with a deepening trend towards the north up to 5000 m This structural configuration has a significant impact on the development of the reservoirs in the basin, with the reservoirs in the north being predominantly associated with Yacoraite Formation and minor Cenozoic units, and those in the south being dominated by Paleozoic reservoir units. The latter is associated with the southward thinning and shallowing of younger units (particularly the Yacoraite and Pirgua deposits, which allocate many reservoirs to the north), which are even absent in many sites.

The stratigraphy of the basin highlights the Mesozoic units, the Yacoraite Formation and the Pirgua Subgroup, as having the greatest potential to function as reservoirs, given their confirmed presence in wells and their petrophysical characteristics, similar to those observed in the Rosario de la Frontera area (southern Santa Bárbara System) by other authors (Chiodi et al. 2014; Invernizzi et al. 2012, C. 2014; Seggiaro et al. 2015; Maffucci et al. 2016; Brender and Kuhn, 2018). Compared to these studies, similar porosity values are observed for the Pirgua Subgroup rocks. This porosity is attributed to a primary condition linked to the lithological characteristics of the unit, mostly composed of sandstones and interbedded conglomerates.

In accordance with the findings of Peralta Arnold et al. (2020), the Yacoraite Formation is hypothesized to function as a prospective geothermal reservoir, exhibiting favorable porosity values and the presence of confined reservoirs, as evidenced by numerous drilling observations. It is a matter of coincidence that Grosso et al. (2013) observed natural fracturing in carbonates of the Yacoraite Formation in the Cerro Amarillo area (northeastern sector of the study basin), identifying three types of fractures with inclinations ranging from 45° to 90° These fractures exhibited optimal secondary porosity and permeability, with matrix permeability of the reservoir ranging from 0.1 to 8.1 mD, and values reaching up to 250 mD. The observed increase in reservoir permeability could be attributed to fractures and microfractures, irrespective of the matrix, which exhibited minimal permeability. Meanwhile, although C. Invernizzi et al. (2014) did not analyze the Yacoraite Formation, they acknowledge that it could significantly contribute to the fractured reservoir volume.

From the W-E and N-S cross-sections (Fig. 3) and the isopach map of the Formation (Fig. 2), a general trend of increasing thickness of the Salta Group toward the east and north can be observed. This trend, combined with a deepening of the Yacoraite Formation's top in the same direction, could help explain the recharge of the aquifers feeding the thermal springs, which are primarily located along the western margin of the SB Mountain Ranges.

As demonstrated in the research by Peralta Arnold et al. (2020), the principal sources of recharge are attributed to elevated topographical zones, namely the Zapla and Cerro Amarillo mountain range, based on the analysis of their isotopic characteristics. The high water table levels give rise to elevated potentiometric surfaces, which in turn regulate the regional recharge of cold meteoric waters. In these areas, the Pirgua and Yacoraite Formations are exposed, and the general eastward deepening of the units would facilitate fluid flow eastward, with surface expression in the hot springs at the foot of the Santa Barbara mountain range.

The spatial analysis of the geothermal gradient revealed significant variations across the basin, with values ranging from 24 °C/km to 40 °C/km (Fig. 6A). If we analyze the described model based on variations in the geothermal gradient, it would be expected that elevated areas controlling the regional recharge of the system would exhibit high lateral flow and the lowest geothermal gradients; areas of intermediate elevation would show regional lateral flow and intermediate geothermal gradients, while areas of low regional topography would correspond to low potentiometric surfaces and regional discharge of warm formation waters from the basin depths, resulting in high geothermal gradients (Hitchon, 1984; Majorowicz et al., 1999; Moeck, 2014). If this was the case, a gradual increase in the geothermal gradient toward the east would be expected, with the highest geothermal gradients occurring near the Santa Bárbara Mountain range. However, the distribution of the basin's geothermal gradient does not follow this pattern (Fig. 6A). Instead, a central zone with a low geothermal gradient is evident, extending through the central part of the basin toward the northern sector. This area separates two high-gradient zones to the east and west. Furthermore, a 10 °C increase in temperature has been observed south of 24 °S, where the gradient increases above 35 °C/km.

Furthermore, when comparing variations of the 50 °C, 100 °C, and 150 °C isotherms in seismic sections (Fig. 3), a correlation is observed between uplifted blocks and an increase in the gradient. This phenomenon could be influenced by a redistribution of heat flow due to regional fluid flow systems driven from areas of high hydraulic charge near the foothills of the Zapla and Cerro Amarillo mountain ranges toward low-elevation areas to the east and north. These fluids, in turn, would circulate through structures of the Salta Group rift to migrate toward zones of lower hydrostatic pressure, as observed in other foreland basins with similar structural configuration (Majorowicz et al., 1999; Weides and Majorowicz, 2014). In summary, the higher vertical Darcy flow velocities in the deep, faulted basin at the foothills of the Zapla and Cerro Amarillo mountain ranges could disrupt vertical heat flow. Finally, another variable that has the capacity to influence the distribution of geothermal gradients is water recharge from the San Francisco River (Fig. 1 and supplementary material 1). This phenomenon results in a reduction of the geothermal gradient in the north-central sector of the basin. Additionally, inverted normal faults exist where recharge occurs through existing fluvial systems (Fig. 1).

6.2. Spatial variation and geological control on heat flow

Heat flow variations are linked to the nature of distinct heat sources, including sediment-derived heat production, upper crustal heat generation, magmatic reservoirs, and radiogenic heat production at variable rates (Springer and Foster, 1998; Springer, 1999; Hamza et al., 2005; Vieira and Hamza, 2014, 2019; Christiansen et al., 2022).

In retro-arc regions, heat flow exhibits an inverse relationship with sediment accumulation in foreland basins. Rapid sedimentation and burial rates significantly reduce HF, as observed in the Sub-Andean region north of 23 °S. Here, high sediment deposition over the last 10 Ma, with subsidence rates of 0.1–0.4 mm/yr (Coudert et al., 1995), results in low heat flow values (~40 mW/m^2) (Springer and Förster, 1998; Springer, 1998). This thermal perturbation can be modeled as heat conduction within a moving medium (Carslaw and Jaeger, 1959). Numerical simulations using typical Andean foreland subsidence rates predict a ~15 % reduction in surface HF across sedimentary sequences (Springer, 1998). In the San Francisco Basin, the Miocene cover thickness decreases north-to-south, from 3000 to 4000 m of Cenozoic fills in the north to 300–700 m in the south—a trend mirrored by Cretaceous-Paleogene strata of the Salta Group. If Cenozoic cover alone explains a 15 % heat flow reduction (Springer, 1998), the expected north-south temperature gradient difference would be ~3 °C/km (with northern values averaging 25 °C/km). However, observed heat flow variations exceed 80 %, implying additional controlling factors.

Upper-crustal heat flow dynamics are poorly constrained in the Central Andes due to the sparse available data. As demonstrated by Springer and Förster (1998) and Springer (1999), a substantial region of elevated heat flow (>90 mW/m^2) was identified, accompanied by the production of a regional heat flow map. Fig. 7A overlays the San Francisco Basin onto the heat flow image by Hamza et al. (2005), revealing a SE-trending zone with values >100 mW/m^2 between 15 °S–30 °S. The basin lies at the SE margin of this anomaly, with heat flow exceeding 80 mW/m^2. The tectonic drivers of this high-heat flow zone remain unclear. While magmatism is concentrated in a narrow, N-S-trending arc

(Altiplano-Puna), regional thermal anomalies suggest either widespread shallow crustal heat sources or deep lithospheric thermal perturbations. This zone aligns with the eastern extent of the Altiplano-Puna Magma Body (APMB) (Ibarra et al. 2019, 2021) which could explain the presence of young (Mio-Pliocene) intermediate magmatic rocks very far from the trench (Maro et al., 2023). Although the Sub-Andean region lacks surface volcanism linked to the APMB, structures like the Lipez fault system may act as lithospheric weak zones, facilitating magma emplacement (Christiansen et al., 2022; Maro et al., 2023) and potentially enhance of the heat flow further east, including the San Francisco Basin. Further evidences are given by the fact that the Central Andean forearc exhibits low-resistivity zones (<10^2 Ω·m), interpreted as permeable, fluid-rich deformation corridors (Schwarz and Kroger, 1997; Yuan et al., 2000; Contreras-Reyes et al., 2021). These regions correlate with upper-plate trans-lithospheric shear zones, where melts accumulate in the back arc and hydrothermal systems develop trenchwards, in direction to the volcanic arc (Contreras-Reyes et al., 2021). Damage zones with high Vp/Vs ratios and concentrated seismicity are likely pathways for magma ascent and hydrothermal fluid migration. Porous-media flow models show fluids migrating laterally beneath dense/impermeable blocks until reaching high-permeability boundaries, where pressure gradients drive focused upward flow (Yañez-Carrizo and Rivera-Herrera, 2019). These zones likely host localized heat flow spikes.

6.3. Preliminary geothermal resource assessment

To assess a preliminary geothermal potential of the Cretaceous Yacoraite Formation in the San Francisco Basin we applied the volumetric deterministic method of Muffler and Cataldi (1978). The approach quantifies the thermal energy stored ("heat in place - HIP") within a defined reservoir volume—comprising porous, permeable rock and fluid—assuming uniform lithological properties (density, heat capacity) and a temperature differential (ΔT) from a usable baseline. The calculation is as follows:

$$\mathrm{HIP} = [\phi\, C_f + (1 - \phi)\, C_r]\; [T_r - T_0]\; A\; h \tag{4}$$

Where ϕ is the effective porosity, C_f and C_r the water and rock matrix heat capacity (J/KgK), respectively, T_r and T_0 the temperature at the top of the reservoir and mean surface temperature (°C), respectively, A the area under consideration (m) and h the net thickness (m). The mean porosity value used for the Yacoraite Formation was 5.7 % (Disalvo 2002; Grosso et al. 2013). The thermal capacity of Yacoraite was derived using the methodology of Huajun (2022), who established regression-based formulas where the variations in thermal properties in carbonate rocks depend mainly on atomic weight and temperature (300–800 K). However, only a fraction of this stored energy is recoverable. The reservoir's total HIP and the extractable portion at wellhead (Extractable Heat, EH) are related through the recovery factor (R_g) as follows:

$$\mathrm{EH} = \mathrm{HIP}\; R_g \tag{5}$$

The recovery factor (Rg) typically ranges from 0.05 to 0.5, depending on reservoir characteristics and extraction technology (Gringarten, 1978; Williams et al. 2008). For uniformly porous, homogeneous reservoirs using liquid-phase injection systems, Rg can approach ~0.5. In contrast, fractured reservoirs - or those planned for single-well (singlet) extraction systems - typically yield lower recovery factors of ~0.1. The existing data on Yacoraite Formation aquifers in the San Francisco Basin indicate that they have a complex lithological and geological structure. This complexity is primarily due to a high level of compartmentalization and fracturing within the unit, likely related to folds, faults, variations in unit thickness, and the intrusion of subvolcanic rocks (Muñoz-Dada et al., 2024). Furthermore, available well logs show poor data on pumping and recovery tests, with some areas exhibiting upwelling confined reservoirs with high flow rates, while others do not. Furthermore, most of the formation waters analyzed exhibit high salinity (Table 1), which could pose challenges for future geothermal exploitation, even though a possible critical elements recovery from the brines might be explored further.

While new and high-quality data on the precise characteristics of the reservoir, recovery times, and water age are needed, we have adopted a conservative recovery factor of 0.15 for the entire basin and the northern sector, and a higher factor of 0.25 for the Caimancito and northern Santa Barbara areas. This distinction reflects the higher density of exploration wells and reliability of the dataset. The calculated geothermal potential values are summarized in Table 3.

These results obtained demonstrate the basin's great potential, where the occurrence of confined aquifers and significant water recharge zones within Zapla and Cerro Amarillo mountain range, generates highly favorable conditions. The increasing thickness of the Yacoraite Formation in the northern area, combined with its increasing depth and temperature, results in an increase in the HIP. This sector boasts the highest density of hydrocarbon exploration wells and the presence of confined aquifers, which gives it greater confidence. A more conservative and smaller area, the Caimancito sector (30 km^2) has been observed to contain six wells with depths exceeding 3000 m of depth, an average reservoir temperature of 149 °C, and a base resource potential of 1304 GJ/m^2, with a conservative recovery potential of 326.02 GJ/m^2. Conversely, although temperatures in the northern sector of the Santa Barbara Sierra are lower (averaging 80 °C), with 11 exploratory wells reaching the Yacoraite Formation at an average depth of 750 m, this area has great potential for further exploration, with base resource values of 2268 GJ/m^2 and a recovery potential of 567 GJ/m^2.

7. Concluding remarks

The architecture of the basin is primarily governed by the tectonic inversion of Cretaceous Salta Rift structures, which creates a complex system of uplifted blocks that dominate the basin margins and provide crucial vertical fluid conduits. The Santa Bárbara Fault plays a major role in the fluid circulation by concentrating most of the thermal springs. A key pivotal ENE-WSW trending rift structure is identified as a significant stratigraphic and geothermal divide, demarcating the separation of northern domains with deep, Meso-Cenozoic reservoirs (e.g., Yacoraite Formation and Pirgua Subgroup) from southern domains dominated by Paleozoic units set at shallower depths.

The petrophysical potential of Yacoraite Formation reservoirs is significant, exhibiting favorable primary and fracture-induced porosity and permeability, as was already proved elsewhere in the region (Disalvo 2002; Grosso et al. 2013). The recharge of these hydrothermal systems is driven by meteoric waters from the topographically elevated Zapla and Cerro Amarillo mountain range, with eastward and northward fluid flow facilitated by the structural and stratigraphic setting of the basin.

The spatial distribution of the geothermal gradient (24–40 °C/km) deviates from classical basin models as the observed thermal anomalies are not solely a consequence of conduction heat flow but are

Table 3
Geothermal potential values.

Region	Area (km^2)	N° of wells	Yacoraite Fm. thickness	Mean T (°C)	HIP (GJ/ m^2)	EH (GJ/ m^2)
Entire basin	3260	37	170.0	98.16	57,753	8663
Northern basin	1746	30	218.2	108.59	45,266	6790
Caimancito	30	6	247.5	149.15	1304	326
Northern Santa Bárbara	118	11	238.2	81.38	2268	567

significantly modulated by the dynamic interplay of complex structure, stratigraphic heterogeneity, and deep fluid circulation within this inverted fault system. In consonance, the variations in heat flow are the result of a complex interplay between multiple geological and thermal processes. While rapid sediment accumulation in the foreland basin exerts primary control in foreland settings, this factor alone is insufficient to account for the observed variability, which exceeds 80 %. The regionally extensive thermal anomaly (>80 mW/m^2) suggests a significant contribution from deeper crustal or lithospheric heat sources, which could be related to the inferred eastern extent of the Altiplano-Puna Magma Body (APMB). In this region, translithospheric fault systems could provide a plausible mechanism for advective heat as well as magma and associated fluid transport far east of the volcanic arc. Consequently, the thermal structure of the region cannot be ascribed to a single cause, rather, it must be regarded as an integrated system where sedimentation patterns, upper crustal heat production, and deep-seated magmatic and/or hydrothermal processes collectively redistribute heat. This highlights the necessity for higher-resolution geothermal data to fully constrain these relationships.

The calculated "heat-in-place" (HIP) values indicate the presence of significant stored thermal energy, thereby confirming the substantial geothermal potential of the Yacoraite Formation within the San Francisco Basin. Future work must prioritize solving the reservoir's hydraulic connectivity, quantifying sustainable flow rates, and addressing the engineering challenges posed by fluid chemistry to accurately constrain the recoverable energy potential.

Funding sources

This contribution was funded by CUIA-CONICET (2023) Italia-Argentina Cooperation Project "Fluid geochemistry and diffuse CO_2 flow as tools for geothermal investigation (Jujuy Province, Argentina): relationship with the tectonic structures and volcanism of the Cretaceous Rift.", by CONICET (PIP 2021–2023 1777), by SeCTER-UNJu (Project FIP 2023 E/G0016), and by the Agencia Nacional de Promoción Científica y Técnica (PICT INVI00796–2021).

CRediT authorship contribution statement

J.P. Villalba Ulberich: Writing – original draft, Visualization, Software, Resources, Methodology, Investigation, Conceptualization. **Y. J. Peralta Arnold:** Writing – original draft, Resources, Formal analysis. **M. Taussi:** Writing – review & editing, Validation, Data curation. **P.J. Caffe:** Writing – review & editing, Supervision, Project administration, Funding acquisition. **F. Tassi:** Writing – review & editing, Validation, Project administration, Funding acquisition.

Declaration of competing interest

The authors declare that they have no known competing financial interests or personal relationships that could have appeared to influence the work reported in this paper.

Acknowledgements

We would like to thank G. Franco (INDyA) and Edgar D. Gonzalez (INECOA) for their assistance with the survey of well data files. We would also like to thank the Secretariat of Mining and Hydrocarbons of the Province of Jujuy for providing us with unpublished information on oil exploration in the basin. The Editor in Chief and two anonymous reviewers are warmly thanked for their constructive comments that helped us to improve this work.

Supplementary materials

Supplementary material associated with this article can be found, in the online version, at doi:10.1016/j.geothermics.2025.103522.

Data availability

Data will be made available on request.

References

Astini, R.A., Marengo, L.F., 2006. Paleoambientes y estratigrafía secuencial de depósitos marinos marginales del Ordovícico de la sierra de Zapla (Sierras Subandinas, noroeste argentino) y su relación con la Cuenca Andina Central. Rev. Geol. Chile 33 (2), 247–276.

Belotti, H.J., Saccavino, L.L., & Schachner, G.A. (1995). Structural styles and petroleum occurrence in the Sub-Andean fold and thrust belt of northern Argentina.

Bianucci, H.A., & JF, H. (1982). Tectogénesis de un sector de la cuenca del subgrupo Pirgua, Noroeste Argentino.

Blackwell, D.D., Steele, J.L., 1989. Thermal conductivity of sedimentary rocks; measurement and significance. In: Naeser, N.D., McCulloh, T.H. (Eds.), Thermal History of Sedimentary Basins; Methods and Case Histories, Vol. 14. Springer, pp. 13–36.

Boll, A., Gómez Omil, R., Hernández, R., 1989. Síntesis Estratigráfica del Grupo Salta. YPF, (inédito), Salta, p. 120.

Brender, N., Kuhn, D., 2018. Feasibility Study For a Medium-Enthalpy Geothermal Power Plant in Rosario de La Frontera. Salta, Argentina.

Brigaud, F., Chapman, D.S., Le Douaran, S., 1990. Estimating thermal conductivity in sedimentary basins using lithologic data and geophysical well logs. AAPG Bull 74 (9), 1459–1477.

Cappetti, G., Giorgi, N., Arias, A., Volpi, G., Rivera, G., Cei, M., Fedeli, M., Di Marzio, G., Pasti, M., Massei, S., Baccarin, F., 2021. The Cerro Pabellón Geothermal Project (Chile): from Surface Exploration to Energy Production, in: Proceeding of the World Geothermal Congress 2020+1. Reykjavik, Iceland.

Carslaw, H.S., Jaeger, J.C., 1959. Conduction of Heat in Solids, 2d ed. Oxford Univ. Press, Oxford, p. 510.

Castillo-Reyes, O., Prol-Ledesma, R.M., Corbo-Camargo, F., Rojas, O., 2024. Geothermal resources in Latin-America and their exploration using electromagnetic methods. Geotherm. Energy 12 (1), 34.

Cecioni, G., 1949. Informe preliminar sobre el levantamento de la zona Sur del anticlinal de Zapla y parte de Santa Bárbara (Provincia de Jujuy). Inst. Geol. Min. 2 (5), 63–75.

Chapman, D.S., Keho, T.H., Bauer, M.S., Picard, M.D., 1984. Heat flow in the Uinta Basin determined from bottom hole temperature (BHT) data. Geophysics 49 (4), 453–466.

Chiodi, A.L., Báez, W.A., Maffucci, R., Viramonte, J.G., Invernizzi, C., Tassi, F., Giordano, G., 2015. Estudio multidisciplinario del sistema geotermal de rosario de la frontera, salta, argentina. J. Appl. Geophy. 88, 83–93.

Christiansen, R.O., Gianni, G.M., Ballivián Justiniano, C.A., García, H.P., Wohnlich, S., 2022. The role of geotectonic setting on the heat flow distribution of southern South America. Geophys. J. Int. 230 (3), 1911–1927.

Cominguez, A.H., Ramos, V.A., 1991. La estructura profunda entre Precordillera y Sierras Pampeanas de la Argentina: evidencias de la sísmica de reflexión profunda. Andean Geology 18 (1), 3–14.

Contreras-Reyes, E., Díaz, D., Bello-González, J.P., Slezak, K., Potin, B., Comte, D., Ruiz, S., 2021. Subduction zone fluids and arc magmas conducted by lithospheric deformed regions beneath the central Andes. Sci. Rep. 11 (1), 23078.

Coudert, L., Frappa, M., Viguier, C., and Arias, R., 1995, Tectonic subsidence and crustal flexure in the Neogene Chaco basin of Bolivia: tectonophysics, v. 243, p. 277–292.

DeCelles, P.G., Giles, K.A., 1996. Foreland basin systems. Basin res. 8 (2), 105–123.

Deming, D., Chapman, D.S., 1988. Heat flow in the Utah-Wyoming thrust belt from analysis of bottom-hole temperature data measured in oil and gas wells. J. Geophys. Res.: Solid Earth 93 (B11), 13657–13672.

Demongodin, L., Pinoteau, B., Vasseur, G., Gable, R., 1991. Thermal conductivity and well logs: a case study in the Paris Basin. Geophys J. Int 105 (3), 675–691.

Disalvo, A., 2002. Cuenca del noroeste: marco geológico y reseña histórica de la actividad petrolera. V Congreso de Exploración y Desarrollo de Hidrocarburos, Mar del Plata. Simp. Rocas Reserv. las Cuencas Product. Argent. 663–677.

Echavarria, L., Hernández, R., Allmendinger, R., Reynolds, J., 2003. Subandean thrust and fold belt of northwestern Argentina: geometry and timing of the Andean evolution. Am. Assoc. Pet. Geol. Bull. 87 (6), 965–985.

Fàbrega Ferrer, E. (2022). Exploration of the next generation of green electricity procurement strategies: evaluation of 24/7 carbon-free electricity and emissionality and their implications for carbon accounting.

Förster, A., Merriam, D.F., Davis, J.C., 1997. Spatial Analysis of Temperature (BHT/DST) Data and Consequences For Heat-Flow Determination in Sedimentary Basins. Geol.

Fuchs, S., Förster, A., 2010. Rock thermal conductivity of Mesozoic geothermal aquifers in the Northeast German Basin. Geochemistry 70, 13–22.

Fuchs, S., Förster, A., 2014. Well-log based prediction of thermal conductivity of sedimentary successions: a case study from the North German Basin. Geophys. J. Int. 196 (1), 291–311.

Fuchs, S., Balling, N., Förster, A., 2015. Calculation of thermal conductivity, thermal diffusivity and specific heat capacity of sedimentary rocks using petrophysical well logs. Geophys. J. Int. 203 (3), 1977–2000.

Fuertes, A., Garcia, R.F., Moya Ruiz, F., Rocha, V., Abraham, C., Dib Ashur, P., 1997. Hoja Hidrogeologica Salta. Mapa Geol. 1 (250.000).

Galli, C.I., Alonso, R.N., Coira, L.B., Herrera Oviedo, E.P., Constantini, O.E., Barrientos Gines, A., Villalba Ulberich, J.P., 2019. Estratigrafía y paleoambientes de los

depósitos del Plioceno de la Cordillera Oriental argentina. Opera Lilloana 52, 367–388.
Galliski, M.A., Viramonte, J.G., 1988. The cretaceous paleorift in northwestern Argentina: a petrologic approach. J. South. Am. Earth. Sci. 1 (4), 329–342.
García, R.F., Rocha Fasola, M.V., Moya Ruiz, F.A., 2008. Los recursos hídricos del sector valles intermontanos de la provincia de Jujuy. In: Relatorio del XVII Congreso Geológico Argentino. Jujuy, Argentina, pp. 556–562.
Gebhard, J.A., Giudici, A.R., Gascón, J.O., 1974. Geología de la Comarca entre el Río Juramento y Arroyo Las Tortugas, provincias de Salta y Jujuy, República Argentina. Rev. Asoc. Geol. Argent 29, 359–376.
Ghassemi, A., 2012. A review of some rock mechanics issues in geothermal reservoir development. Geotech. Geol. Eng. 30 (3), 647–664.
González Villa, R.E., 2002. El Subgrupo Jujuy (Neógeno) Entre Los 24° –26° LS y 64° –66° LO, Tramo Centro Austral de La Cadena Subandina Argentina, Provincias de Salta y Jujuy. Univ. Nac. de Salta, Salta, Argentina. Ph.D. Thesis.
Grant, M., 2013. Geothermal Reservoir Engineering. Elsevier.
Gringarten, A.C., 1978. Reservoir lifetime and heat recovery factor in geothermal aquifers used for urban heating. Pure Appl. Geophys. 117, 297–308.
Grosso, S., López, R., Vergani, G., O'leary, S., 2013. Reservorios carbonáticos naturalmente fracturados en el Yacimiento Caimancito (Formación Yacoraite), cuenca cretácica del noroeste Argentino. Rev. Asoc. Geol. Argent. 70 (1), 53–69.
Hain, M.P., Strecker, M.R., Bookhagen, B., Alonso, R.N., Pingel, H., Schmitt, A.K., 2011. Neogene to quaternary broken foreland formation and sedimentation dynamics in the Andes of NW Argentina (25° S). Tectonics. 30. https://doi.org/10.1029/2010TC002703. TC2006.
Hamza, V.M., Dias, F.J.S., Gomes, A.J., Terceros, Z.G.D., 2005. Numerical and functional representations of regional heat flow in South America. Phys. Earth Planet. Inter. 152 (4), 223–256.
Henry, S.G., Pollack, H.N., 1988. Terrestrial heat flow above the Andean subduction zone in Bolivia and Peru. J. Geophys. Res.: Solid Earth 93 (B12), 15153–15162.
Hernández, R., Disalvo, A., Boll, A., Gómez Omil, R., Galli, C., 1999. Estratigrafía Secuencial del Grupo Salta, con énfasis en las subcuencas de Metán-Alemanía, Noroeste Argentino. Geología del Noroeste Argentino, Relatorio del XIV Congreso Geológico Argentino I, 263–283.
Hitchon, B., 1984. Geothermal gradients, hydrodynamics, and hydrocarbon occurrences, Alberta, Canada. Am. Assoc. Pet. Geol. Bull. 68 (6), 713–743.
Horton, B.K., Folguera, A., 2022. Tectonic inheritance and structural styles in the Andean fold-thrust belt and foreland basin. Andean Structural Styles. Elsevier, pp. 3–28.
Huajun, W., 2022. New approach to the thermal properties of carbonate rocks in geothermal reservoirs: molecular dynamics calculation and case studies. Renew. Energy 198, 861–871.
Ibarra, F., Liu, S., Meeßen, C., Prezzi, C.B., Bott, J., Scheck-Wenderoth, M., Strecker, M. R., 2019. 3D data-derived lithospheric structure of the Central Andes and its implications for deformation: insights from gravity and geodynamic modelling. Tectonophysics. 766, 453–468.
Ibarra, F., Prezzi, C.B., Bott, J., Scheck-Wenderoth, M., Strecker, M.R., 2021. Distribution of temperature and strength in the Central Andean lithosphere and its relationship to seismicity and active deformation. J. Geophys. Res.: Solid Earth 126 (5), e2020JB021231.
IEA, 2025. Global Energy Review 2025. IEA, Paris. https://www.iea.org/reports/global-energy-review-2025. Licence: CC BY 4.0.
Invernizzi, M.C., Pierantoni, P.P., Maffucci, R., Corrado, S., Giordano, G., Viramonte, J., 2012. The geothermal system of Rosario de La Frontera (La Candelaria Ridge-NW Argentina): methods and preliminary results. In: 2st_Scientific_Day_of_The_School_of_Science_and_Technology-Book of Abstracts. UNICAM, pp. 50-50.
Invernizzi, C., Pierantoni, P.P., Chiodi, A., Maffucci, R., Corrado, S., Baez, W., Viramonte, J., 2014. Preliminary assessment of the geothermal potential of Rosario de la Frontera area (Salta, NW Argentina): insight from hydro-geological, hydro-geochemical and structural investigations. J. South. Am. Earth. Sci. 54, 20–36.
IRENA Coalition for Action, 2024. 100% Renewable Energy scenarios: Supporting ambitious Policy Targets. International Renewable Energy Agency, Abu Dhabi.
Izadi, G., Freitag, H.C., 2025. Resource assessment and management for different geothermal systems (hydrothermal, enhanced geothermal, and advanced geothermal systems). Geothermal Energy Engineering. Elsevier, pp. 23–72.
Jolie, E., Scott, S., Faulds, J., Chambefort, I., Axelsson, G., Gutiérrez-Negrín, L.C., Zemedkun, M.T., 2021. Geological controls on geothermal resources for power generation. Nat. Rev. Earth Environ. 2 (5), 324–339.
Jones, C.G., Simmons, S.S., & Moore, J.N. (2025) Characterization of drill core from hydraulically stimulated crystalline rock following hydraulic fracturing at the Utah FORGE geothermal test site.
Kley, J., 1996. Transition from basement-involved to thin-skinned thrusting in the Cordillera Oriental of southern Bolivia. Tectonics. 15 (4), 763–775.
Kley, J., Monaldi, C.R., 2002. Tectonic inversion in the Santa Barbara System of the central Andean foreland thrust belt, northwestern Argentina. Tectonics. 21 (6), 11-1.
Kress, R., 1995. Inverse scattering from an open arc. Math. Methods Appl. Sci. 18 (4), 267–293.
Kukkonen, I.T., Peltoniemi, S., 1998. Relationships between thermal and other petrophysical properties of rocks in Finland. Phys. Chem. Earth 23 (3), 341–349.
Luheshi, M.N., 1983. Estimation of formation temperature from borehole measurements. Geophys. J. Int. 74 (3), 747–776.
Maffucci, R., Bigi, S., Corrado, S., Chiodi, A., Di Paolo, L., Giordano, G., Invernizzi, C., 2015. Quality assessment of reservoirs by means of outcrop data and "discrete fracture network" models: the case history of Rosario de La Frontera (NW Argentina) geothermal system. Tectonophysics. 647–648 (2015), 112–131.
Maffucci, R., Corrado, S., Aldega, L., Bigi, S., Chiodi, A., Di Paolo, L., Invernizzi, C., 2016. Cap rock efficiency of geothermal systems in fold-and-thrust belts: evidence from paleo-thermal and structural analyses in Rosario de La Frontera geothermal area (NW Argentina). J. Volcanol. Geotherm. Res. 328, 84–95.
Majorowicz, J.A., Garven, G., Jessop, A., Jessop, C., 1999. Present heat flow along a profile across the Western Canada Sedimentary Basin: the extent of hydrodynamic influence. Geothermics in Basin Analysis. Springer US, Boston, MA, pp. 61–79.
Maro, G., Suzaño, N.O., Ulberich, J.P.V., Caffe, P.J., Viramonte, J.M., Viramonte, J.G., 2023. Generation of Neogene adakitic-like magmas in the argentine Puna-Eastern Cordillera transition: the Huachichocana subvolcanic complex. Int. J. Earth Sci. 112 (5), 1435–1459.
Marquillas, R.A., Del Papa, C., Sabino, I.F., 2005. Sedimentary aspects and paleoenvironmental evolution of a rift basin: salta Group (Cretaceous–Paleogene), northwestern Argentina. Int. J. Earth Sci. 94, 94–113.
Moeck, I.S., 2014. Catalog of geothermal play types based on geologic controls. Renew. Sustain. Energy Rev. 37, 867–882.
Monaldi, C.R., Boso, M.A., 1987. Dalmanitina (dalmanitina) subandina nov. sp.(trilobita) en la Formacion Zapla del norte argentino. IV Congreso Latinoamericano de Paleontología. St. Cruz Sierra Boliv. (1), 149–157.
Monaldi, C.R., Boso, M.A., Fernández, J.C., 1986. Estratigrafía del Ordovícico de la sierra de Zapla, Pcia. Jujuy. Revista de la Asociación Geológica Argentina 41, 62–69.
Moreno Espelta, C., Arias, J.E., Chávez, A., 1978. Geología Del Área Termal De Reyes, Departamento Capital, Provincia de Jujuy, República Argentina. 3. Revista del Instituto de Ciencias Geológicas. Universidad Nacional de Jujuy, pp. 161–172. Jujuy.
Moreno Espelta, C., Arias, J.E. & Chavez, A., 1981. Geología del área termal de "El Ceibal". Departamento de la Candelaria, Provincia de Salta, República Argentina. Revista del Instituto de Ciencias Geológicas, ISSN 0326-1018. N 4. pp. 85-94.
Muffler, P., Cataldi, R., 1978. Methods for regional assessment of geothermal resources. Geothermics. 7 (2–4), 53–89.
Muñoz Dada, A.C., Maro, G., Caffe, P.J., Villalba Ulberich, J.P., Fracchia, D., 2024. Early Paleogene alkaline magmatism in the Subandean Ranges of Jujuy Province. J. South. Am. Earth. Sci. 149, 105189.
Nguyen, V.G., Sirohi, R., Tran, M.H., Truong, T.H., Duong, M.T., Pham, M.T., Cao, D.N., 2024. Renewable energy role in low-carbon economy and net-zero goal: perspectives and prospects. Energy Environ. 36 (5), 2248–2287. https://doi.org/10.1177/0958305×241253772.
Ortiz, G., Saez, M., Alvarado, P., Rivas, C., García, V., Alonso, R., Zullo, F.M., 2022. Seismotectonic characterization of the 1948 (MW 6.9) Anta earthquake, Santa Bárbara System, central Andes broken foreland of northwestern Argentina. J. South. Am. Earth. Sci. 116, 103822.
Peralta Arnold, Y., Franco, M.G., Tassi, F., Caffe, P.J., Jofre, C.B., Claros, M., Cabassi, J., 2020. Geochemical features of hydrothermal systems in Jujuy Province, Argentina: hints for geothermal fluid exploration. J. South. Am. Earth. Sci. 101, 102627.
Pfiffner, O.A., 2017. Thick-skinned and thin-skinned tectonics: a global perspective. Geosci. (Basel) 7 (3), 71. https://doi.org/10.3390/geosciences7030071.
Quattrocchio, M.E., Borromei, A.M., Deschamps, C.M., Grill, S.C., Zavala, C.A., 2008. Landscape evolution and climate changes in the late pleistocene–Holocene, southern Pampa (Argentina): evidence from palynology, mammals and sedimentology. Quat, Int 181 (1), 123–138. https://doi.org/10.1016/j.quaint.2007.02.018.
Ramos, V.A., 1999. Rasgos estructurales del territorio argentino. Geología Argentina 29 (24), 15–75.
Reiter, M., Jessop, A.M., 1985. Estimates of terrestrial heat flow in offshore eastern Canada. Can. J. Earth. Sci. 22 (10), 1503–1517.
Rahman, A., Farrok, O., Haque, M.M., 2022. Environmental impact of renewable energy source based electrical power plants: solar, wind, hydroelectric, biomass, geothermal, tidal, ocean, and osmotic. Renew. Sustain. Energy Rev. 161, 112279.
Russo, A., 1972. La Estratigrafía Terciaria Del Noroeste argentino. 5° Congreso Geológico Argentino. Villa Carlos Paz, Resúmenes, p. 29.
Russo, A., Serraiotto, A., 1978. Contribución al conocimiento de la estratigrafía terciaria en el noroeste argentino. In: Abstracts: 7° Congreso Geológico Argentino. Neuquén, pp. 715–730.
Ryan, W.B.F., Carbotte, S.M., Coplan, J.O., O'Hara, S., Melkonian, A., Arko, R., Weissel, R.A., Ferrini, V., Goodwillie, A., Nitsche, F., Bonczkowski, J., Zemsky, R., 2009. Global Multi-Resolution Topography synthesis. Geochem. Geophys. Geosyst. 10, Q03014. https://doi.org/10.1029/2008GC002332.
Salfity, J.A., Marquillas, R.A., 1994. Tectonic and sedimentary evolution of the cretaceous-eocene Salta Group basin, Argentina. Cretac. tecton. Andes 266–315.
Schwarz, G., Krueger, D., 1997. Resistivity cross section through the southern central Andes as inferred from magnetotelluric and geomagnetic deep soundings. J. Geophys, Res 102, 11957–11978.
Scott, G.N., 1982. Temperature Equilibration in horeholes: a Statistical Approach. University of Michigan. Unpublished M.*Sc*. thesis.
Seggiaro, R., Aguilera, N., Gallardo, E., Ferreti, J., 1995. Structure and geotermal potential of the Rosario de la Frontera termal área. Salta. Argentina. In: World Geothermal Congress, Actas 2. Florence, Italy, pp. 764–767.
Seggiaro, R., Aguilera, N., Ferretti, J., Gallardo, E., 1997. Estructura del área geotérmica de Rosario de la Frontera, Salta, Argentina. In: 8° Congreso Geológico Chileno. Actas 2. Antofagasta, Chile, pp. 390–394.
Seggiaro, R., Gallardo, E., Aguilera, N., Vitulli, N., Brandan, E., Bercheñi, V., Villagran, A., 2015. Modelo estructural del área termal de la Sierra La Candelaria, departamento Rosario de la Frontera, Salta. Rev. Asoc. Geol. Argent. 72 (2), 265–278.
Shortall, R., Davidsdottir, B., Axelsson, G., 2015. Geothermal energy for sustainable development: a review of sustainability impacts and assessment frameworks. Renew. Sustain. Energy Rev. 44, 391–406.
Springer, M., Förster, A., 1998. Heat-flow density across the Central Andean subduction zone. Tectonophysics. 291 (1–4), 123–139.

Springer, M., 1999. Interpretation of heat-flow density in the Central Andes. Tectonophysics 306 (3–4), 377–395.
Starck, D., 1995, "Silurian-Jurassic stratigraphy and basin evolution of northwestern Argentina", en A. J. Tankard, R. Suarez Soruco y H. J. Welsink, (eds.), Petroleum Basins of South AmericaAAPG Memoir 62, pp. 251–268.
Starck, D., 2011. Cuenca Cretácica-Paleógena del noroeste argentino. *VIII Congreso de Exploración y Desarrollo de Hidrocarburos Simposio Cuencas Argentinas*. Visión Actual, Instituto Argentino del Petróleo y el Gas, pp. 407–453.
Starck, D., Anzótegui, L.M., 2001. The late Miocene climatic change—Persistence of a climatic signal through the orogenic stratigraphic record in Northwestern Argentina. J. S. Am. Earth Sci. 14, 763–774. https://doi.org/10.1016/S0895-9811(01)00066-9.
Taussi, M., Nisi, B., Pizarro, M., Morata, D., Veloso, E.A., Volpi, G., Renzulli, A., 2019. Sealing capacity of clay-cap units above the Cerro Pabellón hidden geothermal system (northern Chile) derived by soil CO2 flux and temperature measurements. J. Volcanol. Geoth. Res. 384, 1–14.
Turner, J.C.M., 1959. Faunas graptolíticas de América del Sur. Rev. Asoc. Geol. Arg. 14 (1–2), 5–211.
Vergani, G., Laffitte, G., Iribarne, M., Apreda, D., 2008. Síntesis de las cuencas productivas de hidrocarburos en el Noroeste de Argentina. VII Congreso de Exploración y Desarrollo De Hidrocarburos (Simposio de Sistemas Petroleros De Las Cuencas Andinas). European Association of Geoscientists & Engineers (pp. cp-266).
Vieira, F.P., Hamza, V.M., 2014. Advances in assessment of geothermal resources of South America. Nat. Resour. 05, 897–913.
Vieira, F., Hamza, V., 2019. Assessment of geothermal resources of South America-a new look. Int. J. Terr. Heat Flow Appl. Geotherm. 2 (1), 46–57.
Villalba Ulberich, J.P., Ercoli, M.D., Alvarez, A., Constantini, O.E., 2021. New insights on landscape and environmental evolution in the Subandean region, Southern Central Andes: sedimentology and geochronology of Guanaco Formation in the Río Chico (Jujuy, Northwestern Argentina). Glob. Planet. Change 207, 103673. https://doi.org/10.1016/j.gloplacha.2021.103673.
Waples, D.W., Ramly, M., 2001. A statistical method for correcting log-derived temperatures. Pet. Geosci. 7 (3), 231–240.
Waples, D.W., Pacheco, J., Vera, A., 2004a. A method for correcting log-derived temperatures in deep wells, calibrated in the Gulf of Mexico. Pet. Geosci. 10 (3), 239–245.
Waples, D.W., Pedersen, M.R., Kuijpers, P., 2004b. Correction of single log-derived temperatures in the Danish Central Graben, North Sea. Nat. Resour. Res. 13 (4), 229–239.
Weides, S., Majorowicz, J., 2014. Implications of spatial variability in heat flow for geothermal resource evaluation in large foreland basins: the case of the Western. Can. Sediment. Basin, Energ. 7 (4), 2573–2594.
Williams, C.F., Reed, M., Mariner, R.H., 2008. A Review of Methods Applied By the US Geological Survey in the Assessment if Identified Geothermal Resources. US Department of Interior, US Geological Survey, p. 27.
Yañez-Carrizo, G., Rivera-Herrera, O., 2019. Crustal dense blocks in the fore-arc and arc region of Chilean ranges and their role in the magma ascent and composition: breaking paradigms in the Andean metallogeny. J. South. Am. Earth. Sci. 93, 51–66.
Yrigoyen, M.R., 1993. The history of hydrocarbons exploration and production in Argentina. J. Pet. Geol. 16 (4), 371–382.
Yuan, X., Sobolev, S., Kind, R., Oncken, O., Bock, G., Asch, G., Schurr, B., Graber, F., Rudloi, A., Hanka, W., Wylegalla, K., Tibi, R., Haberland, C., Rietbrock, A., Giese, P., Wigger, P., Rower, P., Zandt, G., Beck, S., Wallace, T., Pardo, M., Comte, D., 2000. Subduction and collision processes in the Central Andes constrained by converted seismic phases. Nature 408, 958–961.
Zarrouk, S.J., Moon, H., 2014. Efficiency of geothermal power plants: a worldwide review. Geothermics 51, 142–153. https://doi.org/10.1016/j.geothermics.2013.11.001.